

Characteristic Guidance: Non-linear Correction for Diffusion Model at Large Guidance Scale

Candi Zheng^{*1,2} Yuan Lan^{*}

Abstract

Popular guidance for denoising diffusion probabilistic model (DDPM) linearly combines distinct conditional models together to provide enhanced control over samples. However, this approach overlooks nonlinear effects that become significant when guidance scale is large. To address this issue, we propose characteristic guidance, a sampling method that provides first-principle non-linear correction for classifier-free guided DDPMs. Such correction forces the guided DDPMs to respect the Fokker-Planck equation of their underlying diffusion process, in a way that is training-free, derivative-free, and compatible with existing sampling methods. Experiments show that characteristic guidance enhances control and reduces color and exposure issues in image generation, proving effective in diverse applications ranging from latent space sampling to solving physics problems like magnet phase transitions.

1. Introduction

The diffusion model (Sohl-Dickstein et al., 2015; Song & Ermon, 2019; Song et al., 2020b) is a family of generative models that produce high-quality samples by mimicking the diffusion processes of molecules. Denoising diffusion probabilistic model (DDPM) (Ho et al., 2020) is one of the most popular diffusion models whose diffusion process can be viewed as a sequence of denoising steps. It is the core of several large text-to-image models that have been widely adopted in AI art production, such as the latent diffusion model (stable diffusion) (Rombach et al., 2021) and DALL-E (Betker et al., 2023). DDPMs control the generation of samples by learning conditional distributions that are

^{*}Equal contribution ¹Department of Mathematics, Hong Kong University of Science and Technology, Hong Kong SAR, China ²Department of Mechanics and Aerospace Engineering, Southern University of Science and Technology, Shenzhen, China. Correspondence to: Candi Zheng <czhengac@connect.ust.hk>.

Preliminary work. Code available at <https://scraed.github.io/CharacteristicGuidance/>

specified by sample contexts. However, such conditional DDPMs has weak control over context hence do not work well to generate desired content (Luo, 2022).

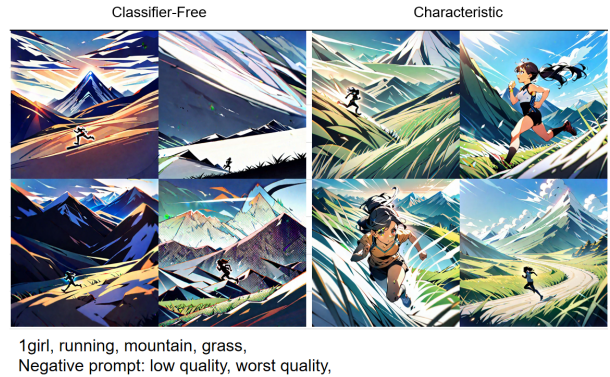


Figure 1. Comparative visualization of images sampled from Stable diffusion XL (Podell et al., 2023) using Classifier Free Guidance versus Characteristic Guidance. Model name: animagineXL 3.0 (CagliostroLab, 2023); Sampler: UniPC (Zhao et al., 2023); Steps: 30; Seeds: 0,1,2,3; Guidance scale: $\omega = 30$.

Guidance techniques, notably classifier guidance (Song et al., 2020b; Dhariwal & Nichol, 2021) and classifier-free guidance (Ho, 2022), providing straightened control at the cost of sample diversity. Classifier guidance, requiring an additional classifier, faces implementation challenges in non-classification tasks like text-to-image generation. Classifier-free guidance circumvents this by linearly combining conditional and unconditional DDPM weighted by a guidance scale parameter. However, this often leads to overly saturated, unnatural images (Ho, 2022) at high control strengths. Despite techniques like dynamic thresholding (Saharia et al., 2022) clipping out-of-range pixel values for color issues, a systematic solution for general sampling tasks, including latent space diffusion (Rombach et al., 2021) and those beyond image generation, remains absent.

This paper proposes a systematic correction for classifier-free guidance at high guidance scales, addressing its theoretical limitation: the neglect of the non-linearity inherent in diffusion models. Instead of combining DDPMs linearly everywhere like classifier-free guidance, characteristic



Figure 2. Comparative visualization of volcano images generated from latent diffusion model using Classifier Free Guidance (CF) versus Characteristic Guidance (CH) without cherry-picking. With increasing guidance scale (ω), CF-guided images exhibit severe color cast and underexposure issues. In contrast, CH guidance produces images with consistent color and exposure. Furthermore, the CH guidance progressively enhances volcanic features such as smoke and lava, while CF guidance remains less responsive to these details.

guidance leverages the characteristic line of the non-linear score Fokker-Planck equation (Lai et al., 2022), effectively brings all combinations back to the initial time ($t=0$) where linear combinations are permitted. Our experiments on Gaussian models demonstrate the clear theoretical advantage of characteristic guidance. Further experiments on Landau-Ginzburg model, Cifar 10 and Imagenet validate its robustness across diverse applications including simulating magnet phase transition and latent space sampling, delivering bias reduction, color/exposure issue fix, and control enhancement.

2. Related Works

2.1. Diffusion Models and Guidance Techniques

Diffusion models, notably Denoising Diffusion Probabilistic Models (DDPMs) (Ho et al., 2020), have become pivotal in generating high-quality AI art (Sohl-Dickstein et al., 2015; Song & Ermon, 2019; Song et al., 2020b). Various guidance methods, including classifier-based (Song et al., 2020b; Dhariwal & Nichol, 2021) and classifier-free techniques (Ho, 2022), have been developed. Recent efforts aim to refine control styles (Bansal et al., 2023; Yu et al., 2023) and enhance sampling quality (Hong et al., 2022; Kim et al., 2022). However, current guidance methods suffer from quality degradation and color saturation issues at high guidance scales. Dynamic thresholding (Saharia et al., 2022) attempts to address this by normalizing quantiles of pixels, but its effectiveness is limited to color-based image pixels, falling short in general tasks like latent space sampling. Community later had to mixing thresholded latents with low guidance scale ones (mcmmonkeyprojects, 2024) to suppress artifacts. Instead of these workarounds, our research aims to address quality issues of classifier-free guidance theoretically and systematically for general tasks, by tackling the non-linear aspects of DDPMs.

2.2. Fokker-Planck Equation and DDPMs

The Fokker-Planck equation is central to the diffusion process in DDPMs (Song et al., 2020b), with efforts to enhance DDPM performance by aligning more closely with this equation showing promise (Lai et al., 2022; Chao et al., 2022). However, traditional approaches face a significant computational hurdle due to the need for complex derivative calculations. Addressing this, our research aims to realign guided DDPMs with the Fokker-Planck in a computationally efficient derivative-free way, thereby leveraging the equation’s benefits while minimizing computational demands.

2.3. Fast Sampling Methods

The significant challenge posed by the slow sampling speed of DDPMs, requiring numerous model evaluations, has spurred the development of accelerated sampling strategies. These strategies range from diffusion process approximations (Song et al., 2020b; Liu et al., 2022; Song et al., 2020a; Zhao et al., 2023) to employing advanced solvers like Runge–Kutta and predictor-corrector methods (Karras et al., 2022; Lu et al., 2022; Zhao et al., 2023). These methods primarily utilize scores or predicted noises for de-noising. Our research focuses on designing a high guidance scale correction that seamlessly integrates with these fast sampling methods, primarily through the modification of scores or predicted noises.

3. Background

3.1. The Denoising Diffusion Probabilistic Model (DDPM)

DDPM models distributions of images $p(\mathbf{x})$ by recovering an original image $\mathbf{x}_0 \sim p(\mathbf{x})$ from one of its noise contaminated versions \mathbf{x}_i . The noise contaminated image is a linear

combination of the original image and a gaussian noise

$$\mathbf{x}_i = \sqrt{\bar{\alpha}_i} \mathbf{x}_0 + \sqrt{1 - \bar{\alpha}_i} \bar{\epsilon}_i; \quad 1 \leq i \leq n, \quad (1)$$

where n is the total diffusion steps, $\bar{\alpha}_i$ is the contamination weight at a time $t_i \in [0, T]$ in the forward diffusion process, and $\bar{\epsilon}_i$ is a standard Gaussian random noise. More detailed information could be found in Appendix A.

The DDPM trains a denoising neural network $\epsilon_\theta(\mathbf{x}, t_i)$ to predict and remove the noise $\bar{\epsilon}_i$ from \mathbf{x}_i . It minimizes the denoising objective (Ho et al., 2020):

$$L(\epsilon_\theta) = \frac{1}{n} \sum_{i=1}^n \mathbf{E}_{\mathbf{x}_0 \sim p(\mathbf{x}), \bar{\epsilon}_i \sim \mathcal{N}(\mathbf{0}, I)} \|\bar{\epsilon}_i - \epsilon_\theta(\mathbf{x}_i, t_i)\|_2^2. \quad (2)$$

The denoising neural network $\epsilon_\theta(\mathbf{x}, t_i)$ notably respects a non-linear score Fokker-Planck equation (37) by being proportional to its solution: $\nabla_{\mathbf{x}_t} \log p(\mathbf{x}_t)$. It is later used in the backward diffusion process to generate image samples from pure Gaussian noises by removing noises step by step (Appendix A).

3.2. Conditional DDPM and Classifier-Free Guidance

Conditional DDPMs, which generate images based on a given condition \mathbf{c} , model the conditional image distribution $p(\mathbf{x}|\mathbf{c})$. One can introduce the dependency on conditions by extending the denoising neural network to include the condition \mathbf{c} , represented as $\epsilon_\theta(\mathbf{x}|\mathbf{c}, t_i)$.

Classifier-free guidance is a technique for conditional image generation that trades off control strength and image diversity. It aims to sample from the distribution (Ho, 2022):

$$p(\mathbf{x}|\mathbf{c}, \omega) \propto p(\mathbf{x}|\mathbf{c})^{1+\omega} p(\mathbf{x})^{-\omega}, \quad (3)$$

where $\omega > 0$ is the guidance scale. When ω is large, the guided DDPM produces samples that have the highest condition likelihood $p(\mathbf{c}|\mathbf{x})$.

Classifier free guidance use the following guided denoising neural network ϵ_{CF} , deduced from (3) using $\epsilon \propto \nabla \log p$, to approximately sample from $p(\mathbf{x}|\mathbf{c}, \omega)$:

$$\epsilon_{CF}(\mathbf{x}|\mathbf{c}, t_i, \omega) = (1 + \omega) \epsilon_\theta(\mathbf{x}|\mathbf{c}, t_i) - \omega \epsilon_\theta(\mathbf{x}, t_i). \quad (4)$$

It exactly computes $\epsilon(\mathbf{x}|\mathbf{c}, t_i, \omega)$, the de-noising neural network of $p(\mathbf{x}|\mathbf{c}, \omega)$, at time $t_i = 0$ (Appendix B). However, it is not a good approximation for most of diffusion time steps $t_i > 0$, especially when the guidance scale ω is large. That is,

$$\epsilon_{CF}(\mathbf{x}|\mathbf{c}, t_i, \omega) \neq \epsilon(\mathbf{x}|\mathbf{c}, t_i, \omega), \quad t_i > 0. \quad (5)$$

This is because $\epsilon(\mathbf{x}|\mathbf{c}, t_i, \omega)$ should respect the same score Fokker-Planck equation (37) as $\epsilon_\theta(\mathbf{x}, t_i)$ and $\epsilon_\theta(\mathbf{x}|\mathbf{c}, t_i)$, hence cannot be their linear combination as the equation is non-linear.

4. Methodology

4.1. The Characteristic Guidance

Our work aims to provide non-linear corrections to the classifier-free guidance, making it approximately satisfy the Fokker-Planck equation in a training-free and derivative-free way. We propose the characteristic guidance as non-linear corrected classifier-free guidance:

$$\epsilon_{CH}(\mathbf{x}|\mathbf{c}, t_i, \omega) = (1 + \omega) \epsilon_\theta(\mathbf{x}_1|\mathbf{c}, t_i) - \omega \epsilon_\theta(\mathbf{x}_2, t_i), \quad (6)$$

in which $\mathbf{x}_1 = \mathbf{x} + \omega \Delta \mathbf{x}$, $\mathbf{x}_2 = \mathbf{x} + (1 + \omega) \Delta \mathbf{x}$, and $\Delta \mathbf{x}$ is a non-linear correction term. It is evident that when $\Delta \mathbf{x} = 0$, the characteristic guidance is equivalent to the classifier-free guidance (4).

We determine the correction $\Delta \mathbf{x}$ from the following non-linear relation:

$$\Delta \mathbf{x} = \mathbf{P} \circ (\epsilon_\theta(\mathbf{x}_2, t_i) - \epsilon_\theta(\mathbf{x}_1|\mathbf{c}, t_i)) \sigma_i, \quad (7)$$

where $\sigma_i = \sqrt{1 - \bar{\alpha}_i}$ is a scale parameter and the operator \mathbf{P} could be an arbitrary orthogonal projection operator. In practice, the equation (7) could be solved with fix-point iteration methods (Appendix D).

The operator \mathbf{P} should be theoretically the identity, but we found that orthogonal projections that serve as regularization greatly accelerates the computation when sampling natural images. For pixel space diffusion model, we suggest the operator \mathbf{P} to be projection from the input to its channel-wise mean. For latent space diffusion model, we suggest the operator \mathbf{P} to be the channel-wise projection to the residual vector $\mathbf{g} = \Delta \mathbf{x} - (\epsilon_\theta(\mathbf{x}, t_i) - \epsilon_\theta(\mathbf{x}|\mathbf{c}, t_i)) \sigma_i$. For low dimensional cases that are not images, we suggest the operator \mathbf{P} to be identity.

4.2. Theoretical Foundation

The characteristic guidance (6) is derived by solving the Fokker Planck equation (37) using the method of characteristics, with classifier-free guidance as the initial condition. Let us consider the case with **infinitesimal** diffusion time steps, define

$$\epsilon(\mathbf{x}, t) = \underset{\epsilon_\theta}{\operatorname{argmin}} L(\epsilon_\theta) \quad (8)$$

as the optimal solution of the DDPM's de-noising objective (2). We propose the Harmonic ansatz assuming that such optimal solution is harmonic:

Ansatz 4.1. *The Harmonic Ansatz: The optimal solution $\epsilon(\mathbf{x}, t)$ is harmonic*

$$\nabla_{\mathbf{x}}^2 \epsilon(\mathbf{x}, t) = 0. \quad (9)$$

This ansatz is inspired by and holds exactly when the distribution of original images $p(\mathbf{x})$ is a Gaussian distribution, and we will show that it works for other cases as well.

Characteristic guidance aims to formulate a new $\epsilon(\mathbf{x}, t)$ by combining two known solutions, $\epsilon_1(\mathbf{x}, t)$ and $\epsilon_2(\mathbf{x}, t)$, under the Harmonic Ansatz. This is elucidated in the following lemma.

Lemma 4.2. *Let $\epsilon(\mathbf{x}, t)$, $\epsilon_1(\mathbf{x}, t)$, and $\epsilon_2(\mathbf{x}, t)$ be optimal solutions of de-noising objectives (2) for three distinct DDPMs, satisfying the Harmonic Ansatz 4.1. Moreover, their initial condition at $t = 0$ satisfies*

$$\epsilon(\mathbf{x}, 0) = (1 + \omega)\epsilon_1(\mathbf{x}, 0) - \omega\epsilon_2(\mathbf{x}, 0), \quad (10)$$

where ω is a constant. Then, we have the relation

$$\epsilon(\mathbf{x}, t) = (1 + \omega)\epsilon_1(\mathbf{x} + \omega\Delta\mathbf{x}, t) - \omega\epsilon_2(\mathbf{x} + (1 + \omega)\Delta\mathbf{x}, t), \quad (11)$$

where $\Delta\mathbf{x}$ is given by

$$\Delta\mathbf{x} = (\epsilon_2(\mathbf{x} + (1 + \omega)\Delta\mathbf{x}, t) - \epsilon_1(\mathbf{x} + \omega\Delta\mathbf{x}, t))\sigma(t), \quad (12)$$

in which $\sigma(t) = \sqrt{1 - e^{-t}}$ for $t \in [0, T]$ be the time of forward diffusion process.

Replacing ϵ , ϵ_1 , and ϵ_2 with $\epsilon_{CH}(\mathbf{x}|\mathbf{c}, t_i, \omega)$, $\epsilon_\theta(\mathbf{x}|\mathbf{c}, t_i)$, and $\epsilon_\theta(\mathbf{x}, t_i)$ gives us the characteristic guidance. The detailed argument for lemma 4.2 and the connection between $\sigma(t)$ and σ_i are established in Appendix E.

The characteristic guidance applies the classifier-free guidance only at the initial condition $t_0 = 0$ by (10), and then solves the Fokker-Planck equation under the harmonic ansatz for the rest of the diffusion process. This allows us to use the classifier-free guidance when it is most accurate and avoid its drawbacks later on.

5. Experiments

5.1. Conditional Gaussian: Where the Harmonic Ansatz Holds Exactly

We compare the performance of classifier-free guidance and characteristic guidance on sampling from conditional 2D Gaussian distributions, a scenario where the harmonic ansatz is exact.

In this experiment, we set two DDPMs analytically (Appendix F) for two Gaussian distribution: the conditional distribution $p(\mathbf{x}|\mathbf{c})$ and the unconditional distribution $p(\mathbf{x})$

$$\begin{aligned} p(\mathbf{x}|\mathbf{c}) &= \mathcal{N}(x_1, x_2 | (c_1, c_2)^T, I) \\ p(\mathbf{x}) &= \mathcal{N}(x_1, x_2 | (0, 0)^T, 5I) \end{aligned} \quad (13)$$

The guided diffusion model (33) aims to sample from the distribution (3), which is another 2D Gaussian distribution for x_1, x_2 whose contour is plotted in Fig.3. The harmonic ansatz holds exactly for Gaussian distributions because their score functions are harmonic, so as the corresponding DDPMs modeling them.

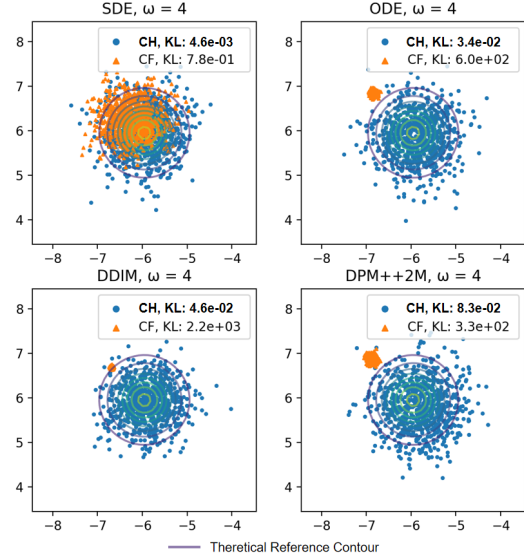


Figure 3. Samples and the KL divergence from characteristic guidance (CH) and classifier free guidance (CF) guided DDPM modeling conditional Gaussian distribution. The contours corresponds to the theoretical reference (ground truth) distribution of the guided DDPM (3).

Samples from the classifier-free guidance and characteristic guidance at $c_1 = -5, c_2 = 5, \omega = 4$ are shown in Fig.3. More results could be found in Fig.9. The projection operator \mathbf{P} for characteristic guidance is set to be identity. Four different sampling methods are tested: the SDE (29) (1000 steps), probabilistic ODE (Song et al., 2020b) (1000 steps), DDIM (Song et al., 2020a) (20 steps), and DPM++2M (Lu et al., 2022) (20 steps). These samples are compared with the theoretical reference distribution (3) using Kullback–Leibler(KL) divergence, which is calculated by assuming the samples are also Gaussian distributed.

Fig.3 shows that characteristic guidance achieves better KL divergence than classifier-free guidance for every sampling methods. It worth noting that classifier-free guidance suffers from severe bias and catastrophic loss of diversity when ODE based sampling methods (ODE, DDIM, and DPM++2M) are used. Contrarily, characteristic guidance always yields correct sampling with KL divergence better than classifier-free guidance’s best SDE samples. In conclusion, characteristic guidance is capable of reducing bias, increase diversity, and eliminating the performance gap between ODE and SDE sampling methods for analytically defined DDPMs when the harmonic ansatz holds exactly.

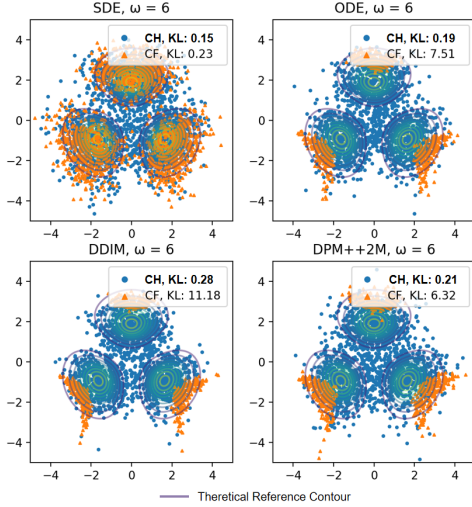


Figure 4. Comparison between characteristic guidance (CH) and classifier free guidance (CF) guided DDPM on modeling mixture of Gaussian distribution. The contours corresponds to the theoretical reference distribution of the guided DDPM (3). Samples from characteristic guidance shows better KL divergence than those from classifier-free guidance.

5.2. Mixture of Gaussian: Where the Harmonic Ansatz Holds Roughly

We compare the performance of classifier-free guidance and characteristic guidance on sampling from Mixture of Gaussian distributions. In this case, the harmonic ansatz is a good approximation for most of the region except where the components overlap significantly.

We train conditional and unconditional DDPM to learn two distributions: The conditional distribution $p(\mathbf{x}|\mathbf{c})$

$$p(\mathbf{x}|\mathbf{c}) = \prod_{i=0}^2 \mathcal{N}(\mathbf{x}|\boldsymbol{\mu}_i, I)^{c_i}, \quad (14)$$

where $\mathbf{c} = (c_0, c_1, c_2)^T$ is a three dimensional one-hot vector, $\boldsymbol{\mu}_0 = (-1, -1/\sqrt{3})^T$, $\boldsymbol{\mu}_1 = (1, -1/\sqrt{3})^T$, $\boldsymbol{\mu}_2 = (0, \sqrt{3} - 1/\sqrt{3})^T$, and the unconditional distribution $p(\mathbf{x})$

$$p(\mathbf{x}) = \frac{1}{3} \sum_{\{\mathbf{e}_i, i=0,1,2\}} p(\mathbf{x}|\mathbf{e}_i) \quad (15)$$

where $\{\mathbf{e}_i, i = 0, 1, 2\}$ represents all one-hot vectors in three dimension space. The guided diffusion model is again aims to sample from the distribution (3), whose contour is plotted in Fig.4.

Samples from the classifier-free guidance and characteristic guidance at $\omega = 6$ are shown in Fig.4. For characteristic guidance, the projection operator \mathbf{P} is set to be identity.

More results could be found in Fig.58. Four different sampling methods are tested: the SDE (1000 steps), probabilistic ODE (1000 steps), DDIM (20 steps), and DPM++2M (20 steps). Samples are compared with the theoretical reference distribution (3) using Kullback–Leibler(KL) divergence, which is calculated by assuming the sample distribution is another mixture of Gaussian with each components are Gaussian distributed.

Fig.4 shows that the classifier-free guidance again suffers from bias and significantly loss of diversity when ODE based sampling methods (ODE, DDIM, and DPM++2M) are used. Contrarily, samples from characteristic guidance has less bias, better diversity, and smaller performance gap between ODE and SDE. However, these samples has less clear boundaries between components than the theoretical reference contour. This is because the harmonic ansatz is not valid in the overlap regions. Besides, minor artifacts appears because iterating on trained neural networks ϵ brings in approximation errors. Nonetheless, characteristic guidance is still capable of reducing bias, improve diversity, and reduce the performance gap between ODE and SDE sampling methods when the harmonic ansatz holds roughly.

5.3. Cooling of the Magnet: Where the Harmonic Ansatz Not Supposed to Hold

Guidance can be interpreted as a cooling process in physics with the guidance scale ω representing the temperature drop. We demonstrate that guidance can simulate the cooling of a magnet around the Curie temperature, at which a paramagnetic material gains permanent magnetism through phase transition. Such transition is a consequence of 3rd order terms in score function, where the harmonic ansatz does not hold.

Suppose we have a square slice of 2-dimensional paramagnetic material which can be magnetized only in the direction perpendicular to it. It can be further divided uniformly into 8×8 smaller pieces, with each pieces identified by its index (i, j) . We use a scalar field $\phi_{i,j}$ to record the magnitude of magnetization of each piece, which can be viewed as a single channel 8×8 image of magnetization.

The probability of observing a particular configuration of ϕ , according to statistical physics, is proportional to the Boltzmann distribution

$$p(\phi; T) \propto e^{-\beta H(\phi; T)}, \quad (16)$$

where $\beta H(\phi; T)$ is Hamiltonian at temperature T , assigning an energy to each of possible ϕ . At temperature near the Curie temperature T_c , a Landau-Ginzburg model (Kardar, 2007) of magnet uses a Hamiltonian (60) (Appendix H) with 4-th order terms. Such terms are the key to characterise phase transition of magnet, but its gradient (score function) is a third order term that does not respect the harmonic

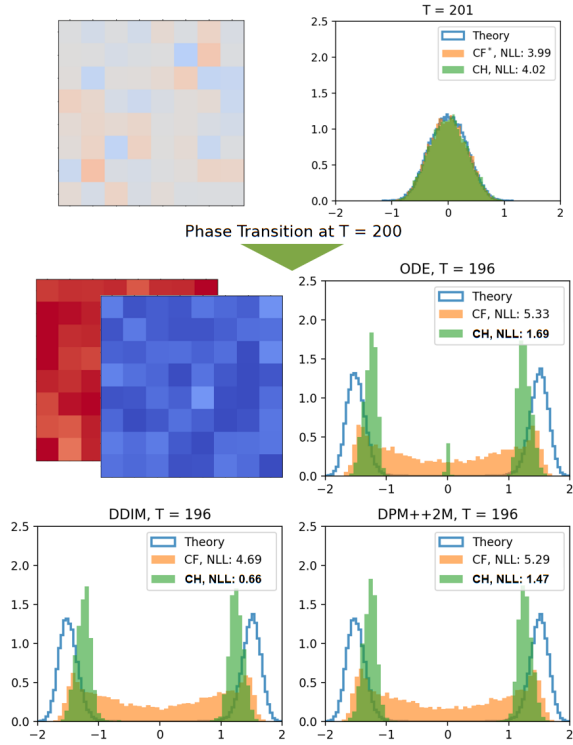


Figure 5. Comparison between characteristic guidance (CH) and classifier free guidance (CF) guided DDPM on simulating magnet cooling. The images in the upper and middle left (blue and red lattices) depict samples from DDPMs, while the histograms illustrate the distribution of samples’ mean value (magnetization) across different temperatures. The contours corresponds to the theoretical reference distribution of magnetization. The characteristic guidance has better NLL and is more capable in capturing peak separation of sample magnetization.

ansatz.

A remarkable property about the Landau-Ginzburg model, bearing surprising similarity with the DDPM guidance (3), is

$$p(\phi; (1 + \omega)T_1 - \omega T_0) \propto p(\phi; T_1)^{1+\omega} p(\phi; T_0)^{-\omega}, \quad (17)$$

where $\omega > 0$ is the guidance scale, $T_1 > T_0$ are two distinct temperature. This means if we know the distribution of our magnet at two distinct temperatures T_0 and T_1 , we know its distribution at any temperature cooler than T_1 by adjusting the guidance scale ω .

We train a conditional DDPM simulating the cooling of a magnet with the Curie temperature $T_c = 200$. The model is trained at two distinct temperatures $p(\phi|T_1 = 201)$ and $p(\phi|T_0 = 200)$, corresponds to $\omega = 0$ and $\omega = 1$. Samples at lower temperatures $T = 196$ ($\omega = 5$) are later obtained by adjusting the guidance scale. Four different sampling

methods are tested: the SDE (1000 steps), probabilistic ODE (1000 steps), DDIM (20 steps), and DPM++2M (20 steps). The projection operator \mathbf{P} for characteristic guidance is set to be the channel-wise mean. Samples are generated again in four different ways: the SDE, probabilistic ODE, DDIM, and DPM++2M. The histogram of the mean value of the magnetization ϕ field values are plotted in Fig.5. More results are plotted in Fig.11.

Fig.5 demonstrates the phase transition. Above the Curie temperature $T_c = 200$, the histogram of the mean magnetization has one peak centered at 0. Below the Curie temperature, the histogram of the mean magnetization has two peaks with non-zero centers. Such changes in the number of peaks represents a phase change from non-magnet to a permanent magnet.

Characteristic guidance outperforms classifier-free guidance in sample quality below the Curie temperature, showcasing better negative log-likelihood (NLL) and effectively capturing distinct peaks in magnetization of samples. In contrast, classifier-free guidance struggles to produce distinct peaks. Despite its biased peak positions compared with theoretical expectations, characteristic guidance still demonstrates superior performance in modeling phase transitions, where the harmonic ansatz does not hold.

5.4. Cifar 10: Natural Image Generation

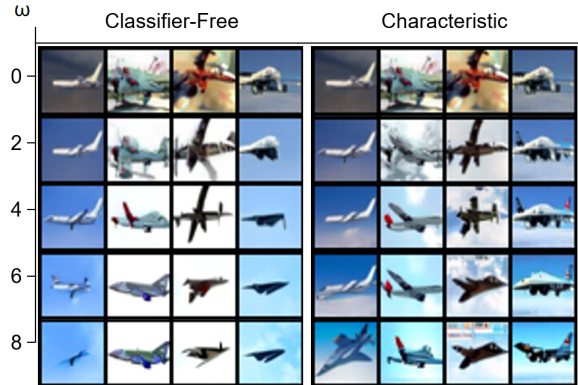


Figure 6. Comparative visualization of aircraft images generated from DDPM using Classifier Free Guidance (CF) versus Characteristic Guidance (CH). With increasing guidance scale (ω), the images guided by CF tend to have dull or even white backgrounds. However, the images guided by CH have more vivid and realistic backgrounds with sky and clouds.

We compare the performance of classifier-free guidance and characteristic guidance on generating natural images with DDPM trained on the Cifar 10 dataset. The quality of generated image are evaluated by the Frechet Inception Distance (FID) (Heusel et al., 2017), the Inception Score (IS) (Salimans et al., 2016) and visual inspection.

Aircraft images generated by both classifier-free and characteristic guidance are compared in Fig.6 at various guidance scales. We fix the initial random noise for both classifier-free and characteristic guided DDPMs, therefore samples at small ω have same context. However, for large guidance scale ω , images generated by classifier-free guidance tend to have dull or even white backgrounds, while images guided by characteristic guidance have more vivid and realistic backgrounds with sky and clouds. This means characteristic guidance is less biased in color than classifier-free guidance.

Table 1. FID and IS of characteristic guidance (CH) and classifier free guidance (CF) guided DDPM on Cifar10 dataset. Samples are drawn with DDIM and DPM++2M methods. Characteristic guidance achieves similar IS with classifier-free guidance while significantly enhance the FID when the guidance scale ω is large.

ω	DDIM			
	FID		IS	
	CF	CH	CF	CH
0.3	4.52	4.46	9.18	9.23
0.6	4.80	4.64	9.39	9.43
1.0	6.22	5.86	9.52	9.53
1.5	8.56	7.89	9.50	9.57
2.0	11.02	10.10	9.49	9.51
4.0	19.85	18.15	9.23	9.22
6.0	27.04	24.77	8.85	8.86
ω	DPM++2M			
	FID		IS	
	CF	CH	CF	CH
0.3	3.33	3.35	9.69	9.69
0.6	3.51	3.44	9.93	9.93
1.0	4.75	4.51	10.06	10.04
1.5	6.85	6.37	10.08	10.07
2.0	9.11	8.34	10.04	10.04
4.0	17.04	15.52	9.75	9.76
6.0	23.47	21.46	9.33	9.38

The evaluation metrics for sample quality are listed in Table.1, highlighting that characteristic guidance typically yields samples with lower FID and comparable IS to classifier-free guidance. Two fast sampling methods are tested: DDIM (50 steps), and DPM++2M (50 steps), with the operator \mathbf{P} for characteristic guidance to be projection from the input to its channel-wise mean. FID assesses the discrepancy between sample and dataset distributions, whereas IS evaluate the InceptionV3 model’s classification results on these samples. Consequently, characteristic guidance appears more effective in stimulating the InceptionV3 model with features that align closely with the original dataset, causing significant FID drop.

5.5. ImageNet 256: Correction for Latent Space Model

The characteristic guidance works on latent space diffusion models (LDM) (Rombach et al., 2021) in a different way: it enhances the control strength rather than lowering the FID. We test the characteristic guidance on the LDM for ImageNet256 dataset, with codes and models adopted from (Rombach et al., 2021). The quality of generated image are evaluated by the Frechet Inception Distance (FID), the Inception Score (IS) and visual inspection.

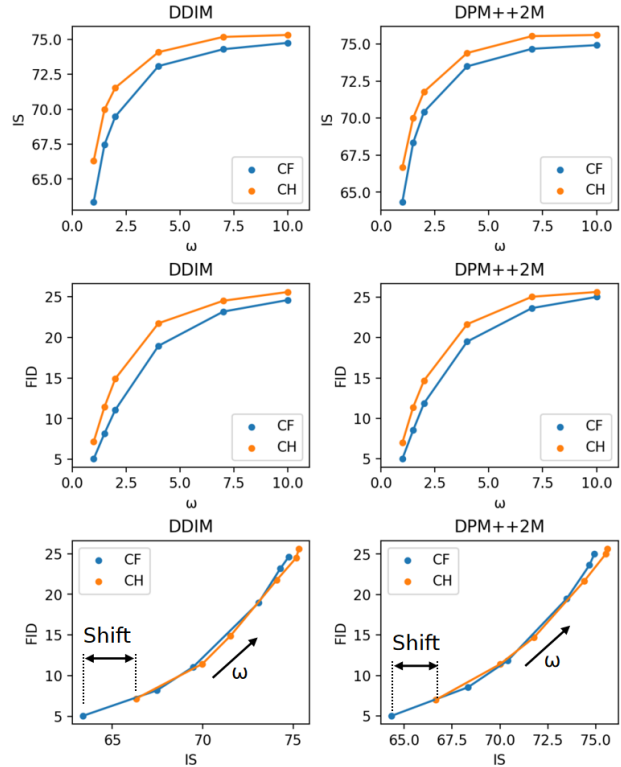


Figure 7. Comparison of FID and IS between characteristic guidance (CH) and classifier free guidance (CF) guided DDPM on ImageNet256 dataset. Samples are drawn with DDIM and DPM++2M (not completed, it is now copied from DDIM results) methods from latent diffusion model. Characteristic guidance achieves better IS than classifier-free guidance but worse FID. However, the IS-FID curve of CH and CF guidance coincide with each other.

In Fig.2, we compare volcano images generated using both classifier-free and characteristic guidance across various guidance scales. For both methods, we maintained consistent initial random noise, ensuring that samples at smaller ω values share similar contexts. However, at larger guidance scales ω , images guided by the classifier-free method show notable color distortion and underexposure. In contrast, characteristic guidance maintains color consistency and proper exposure, progressively accentuating volcanic

features like smoke and lava. This comparison highlights characteristic guidance’s capability in latent space, effectively mitigating color issues, addressing exposure problems, and enhancing context control.

In Fig.7, we present sample quality evaluation metrics using two fast sampling methods: DDIM (50 steps) and DPM++2M (50 steps). Characteristic guidance, while improving the Inception Score (IS), adversely impacts the Fréchet Inception Distance (FID) compared to classifier-free guidance. This IS-FID trade-off complicates the evaluation of which guidance performs better. Surprisingly, the IS-FID curves of both methods align closely, with the curve for characteristic guidance showing a rightward shift. This shift implies that characteristic guidance achieves higher IS at lower guidance scales, effectively operating at a higher effective guidance scale ω than classifier-free guidance, suggesting enhanced control strength.

The differing functionality of characteristic guidance on Cifar10 and ImageNet may be attributed to our choice of projection operator \mathbf{P} . In latent space, we use channel-wise projection to the residual vector, not to the channel-wise mean, as the latter’s correction on RGB color does not make sense in latent space. Despite the unclear interpretation of this approach in latent space, our results suggest a significant correlation with control strength and the guidance scale ω .

5.6. Stable Diffusion

We have successfully integrated our characteristic guidance into Stable Diffusion WebUI (AUTOMATIC1111, 2023) as extension, supporting all existing samplers provided in it. Fig.1 showcases a comparative visualization of images from Stable Diffusion XL (Podell et al., 2023). More visualizations could be found in Appendix. Characteristic guidance not only resolves exposure issues but also more closely aligns with prompts compared to classifier-free guidance.

6. Discussion

6.1. The Stopping Criteria for Iteration

Characteristic guidance provides non-linear correction by solving (7) iteratively. Such iteration happens for every time step and is controlled by a threshold (tolerance η of residual in Appendix.D) and a maximal iteration number (set to 10) as the stopping criteria. We exam how the threshold affects evaluation metrics (FID and IS) and the total number of iteration, which heavily affects the computational efficiency because each iteration calls the de-noising neural network.

Fig.8 illustrates the relationship between various threshold levels (parameter η in Appendix.D) and their corresponding effects on Fréchet Inception Distance (FID) and Inception Score (IS). It is observed that convergence is typically at-

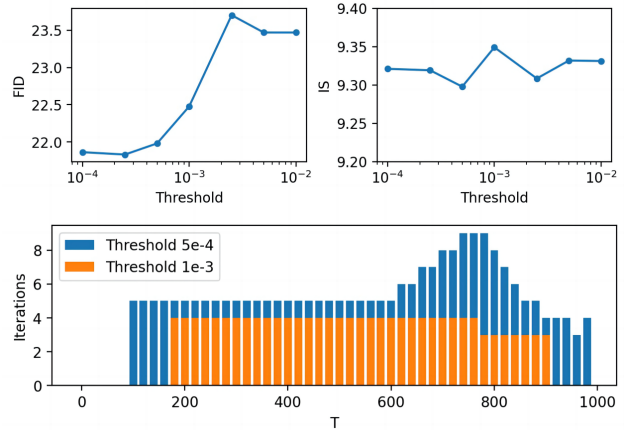


Figure 8. Convergence and iteration analysis on Cifar10 dataset ($\omega = 6$, DPM, 50 steps). The graph shows the relationship between threshold levels and their effects on Fréchet Inception Distance (FID) and Inception Score (IS). It also plots the iteration count of characteristic guidance, for a typical generation process, across various thresholds against diffusion time step T , ranging from 0 (image) to 1000 (noise).

tained at thresholds lower than $1e^{-3}$. Additionally, the chart also displays the number of iterations employed by characteristic guidance at different thresholds, plotted against the diffusion time step T , which varies from 0 (image) to 1000 (noise). It shows that the non-linear corrections mainly take place at the middle of the diffusion process, which is known to be a critical stage for context generation (Zhang et al., 2023).

7. Conclusion

We introduced characteristic guidance, a new guidance method providing non-linear correction to classifier-free guided DDPMs. We evaluated characteristic guidance across various scenarios, such as conditional Gaussian, mixture of Gaussian, the Landau-Ginzburg model for magnets, Cifar10, and Imagenet. The results demonstrate its effectiveness in reducing bias and enhancing control. It is, as far as we know, the first attempt to lay the theoretical groundwork for large guidance scale correction.

Limitations The process of resolving the non-linear correction (7) requires iterative computations involving neural networks. This approach, without effective regularization, tends to be slow. Exploring advanced regularization techniques beyond the projection \mathbf{P} could enhance the convergence rate hence accelerate the computation.

References

- Anderson, B. D. O. Reverse-time diffusion equation models. *Stochastic Processes and their Applications*, 12:313–326, 1982. URL <https://api.semanticscholar.org/CorpusID:3897405>.
- AUTOMATIC1111. Stable diffusion webui, 2023. URL <https://github.com/AUTOMATIC1111/stable-diffusion-webui>.
- Bansal, A., Chu, H.-M., Schwarzschild, A., Sengupta, S., Goldblum, M., Geiping, J., and Goldstein, T. Universal guidance for diffusion models. *2023 IEEE/CVF Conference on Computer Vision and Pattern Recognition Workshops (CVPRW)*, pp. 843–852, 2023. URL <https://api.semanticscholar.org/CorpusID:256846836>.
- Betker, J., Goh, G., Jing, L., Brooks, T., Wang, J., Li, L., Ouyang, L., Zhuang, J., Lee, J., Guo, Y., et al. Improving image generation with better captions, 2023.
- CagliostroLab. Animate xl 3.0, 2023. URL <https://huggingface.co/cagliostroLab/animate-xl-3.0>.
- Chao, C.-H., Sun, W.-F., Cheng, B. W., and Lee, C.-Y. On investigating the conservative property of score-based generative models. In *International Conference on Machine Learning*, 2022. URL <https://api.semanticscholar.org/CorpusID:256105781>.
- Dhariwal, P. and Nichol, A. Diffusion models beat gans on image synthesis. *ArXiv*, abs/2105.05233, 2021. URL <https://api.semanticscholar.org/CorpusID:234357997>.
- Heusel, M., Ramsauer, H., Unterthiner, T., Nessler, B., and Hochreiter, S. Gans trained by a two time-scale update rule converge to a local nash equilibrium. In *Neural Information Processing Systems*, 2017. URL <https://api.semanticscholar.org/CorpusID:326772>.
- Ho, J. Classifier-free diffusion guidance. *ArXiv*, abs/2207.12598, 2022. URL <https://api.semanticscholar.org/CorpusID:249145348>.
- Ho, J., Jain, A., and Abbeel, P. Denoising diffusion probabilistic models. *ArXiv*, abs/2006.11239, 2020. URL <https://api.semanticscholar.org/CorpusID:219955663>.
- Hong, S., Lee, G., Jang, W., and Kim, S. W. Improving sample quality of diffusion models using self-attention guidance. *ArXiv*, abs/2210.00939, 2022. URL <https://api.semanticscholar.org/CorpusID:252683688>.
- Kardar, M. *Statistical fields*, pp. 19–34. Cambridge University Press, 2007. doi: 10.1017/CBO9780511815881.003.
- Karras, T., Aittala, M., Aila, T., and Laine, S. Elucidating the design space of diffusion-based generative models. *ArXiv*, abs/2206.00364, 2022. URL <https://api.semanticscholar.org/CorpusID:249240415>.
- Kim, D., Kim, Y., Kang, W., and Moon, I.-C. Refining generative process with discriminator guidance in score-based diffusion models. In *International Conference on Machine Learning*, 2022. URL <https://api.semanticscholar.org/CorpusID:254096299>.
- Lai, C.-H., Takida, Y., Murata, N., Uesaka, T., Mitsufuji, Y., and Ermon, S. Fp-diffusion: Improving score-based diffusion models by enforcing the underlying score fokker-planck equation. In *International Conference on Machine Learning*, 2022. URL <https://api.semanticscholar.org/CorpusID:259164358>.
- Langley, P. Crafting papers on machine learning. In Langley, P. (ed.), *Proceedings of the 17th International Conference on Machine Learning (ICML 2000)*, pp. 1207–1216, Stanford, CA, 2000. Morgan Kaufmann.
- Liu, L., Ren, Y., Lin, Z., and Zhao, Z. Pseudo numerical methods for diffusion models on manifolds. *ArXiv*, abs/2202.09778, 2022. URL <https://api.semanticscholar.org/CorpusID:247011732>.
- Lu, C., Zhou, Y., Bao, F., Chen, J., Li, C., and Zhu, J. Dpm-solver++: Fast solver for guided sampling of diffusion probabilistic models. *ArXiv*, abs/2211.01095, 2022. URL <https://api.semanticscholar.org/CorpusID:253254916>.
- Luo, C. Understanding diffusion models: A unified perspective. *ArXiv*, abs/2208.11970, 2022. URL <https://api.semanticscholar.org/CorpusID:251799923>.
- mcmonkeyprojects. sd-dynamic-thresholding: A dynamic thresholding method for stable diffusion, 2024. URL <https://github.com/mcmonkeyprojects/sd-dynamic-thresholding>.
- Podell, D., English, Z., Lacey, K., Blattmann, A., Dockhorn, T., Müller, J., Penna, J., and Rombach, R. Sdxl: Improving latent diffusion models for high-resolution image synthesis, 2023.

- Rombach, R., Blattmann, A., Lorenz, D., Esser, P., and Ommer, B. High-resolution image synthesis with latent diffusion models. *2022 IEEE/CVF Conference on Computer Vision and Pattern Recognition (CVPR)*, pp. 10674–10685, 2021. URL <https://api.semanticscholar.org/CorpusID:245335280>.
- Saharia, C., Chan, W., Saxena, S., Li, L., Whang, J., Denton, E., Ghasemipour, S. K. S., Ayan, B. K., Mahdavi, S. S., Lopes, R. G., Salimans, T., Ho, J., Fleet, D. J., and Norouzi, M. Photorealistic text-to-image diffusion models with deep language understanding, 2022.
- Salimans, T., Goodfellow, I. J., Zaremba, W., Cheung, V., Radford, A., and Chen, X. Improved techniques for training gans. *ArXiv*, abs/1606.03498, 2016. URL <https://api.semanticscholar.org/CorpusID:1687220>.
- Sohl-Dickstein, J. N., Weiss, E. A., Maheswaranathan, N., and Ganguli, S. Deep unsupervised learning using nonequilibrium thermodynamics. *ArXiv*, abs/1503.03585, 2015. URL <https://api.semanticscholar.org/CorpusID:14888175>.
- Song, J., Meng, C., and Ermon, S. Denoising diffusion implicit models. *ArXiv*, abs/2010.02502, 2020a. URL <https://api.semanticscholar.org/CorpusID:222140788>.
- Song, Y. and Ermon, S. Generative modeling by estimating gradients of the data distribution. In *Neural Information Processing Systems*, 2019. URL <https://api.semanticscholar.org/CorpusID:196470871>.
- Song, Y., Sohl-Dickstein, J. N., Kingma, D. P., Kumar, A., Ermon, S., and Poole, B. Score-based generative modeling through stochastic differential equations. *ArXiv*, abs/2011.13456, 2020b. URL <https://api.semanticscholar.org/CorpusID:227209335>.
- Uhlenbeck, G. E. and Ornstein, L. S. On the theory of the brownian motion. *Physical Review*, 36:823–841, 1930. URL <https://api.semanticscholar.org/CorpusID:121805391>.
- Vincent, P. A connection between score matching and denoising autoencoders. *Neural Computation*, 23:1661–1674, 2011. URL <https://api.semanticscholar.org/CorpusID:5560643>.
- Walker, H. F. and Ni, P. Anderson acceleration for fixed-point iterations. *SIAM J. Numer. Anal.*, 49:1715–1735, 2011. URL <https://api.semanticscholar.org/CorpusID:4527816>.
- Yang, L., Zhang, Z., Hong, S., Xu, R., Zhao, Y., Shao, Y., Zhang, W., Yang, M.-H., and Cui, B. Diffusion models: A comprehensive survey of methods and applications. *ACM Computing Surveys*, 2022. URL <https://api.semanticscholar.org/CorpusID:252070859>.
- Yu, J., Wang, Y., Zhao, C., Ghanem, B., and Zhang, J. Freedom: Training-free energy-guided conditional diffusion model. *ArXiv*, abs/2303.09833, 2023. URL <https://api.semanticscholar.org/CorpusID:257622962>.
- Zhang, Z., Zhao, Z., Yu, J., and Tian, Q. Shift-dpms: Exploring conditional diffusion models by shifting diffusion trajectories. *ArXiv*, abs/2302.02373, 2023. URL <https://api.semanticscholar.org/CorpusID:256615850>.
- Zhao, W., Bai, L., Rao, Y., Zhou, J., and Lu, J. Unipc: A unified predictor-corrector framework for fast sampling of diffusion models. *ArXiv*, abs/2302.04867, 2023. URL <https://api.semanticscholar.org/CorpusID:256697404>.

A. The Denoising Diffusion Probabilistic Model (DDPMs)

DDPMs (Ho et al., 2020) are models that generate high-quality images from noise via a sequence of denoising steps. Denoting images as random variable \mathbf{x} of the probabilistic density distribution $p(\mathbf{x})$, the DDPM aims to learn a model distribution that mimics the image distribution $p(\mathbf{x})$ and draw samples from it. The training and sampling of the DDPM utilize two diffusion process: the forward and the backward diffusion process.

The forward diffusion process of the DDPM provides necessary information to train a DDPM. It gradually adds noise to existing images $\mathbf{x}_0 \sim p(\mathbf{x})$ using the Ornstein–Uhlenbeck diffusion process (OU process) (Uhlenbeck & Ornstein, 1930) within a finite time interval $t \in [0, T]$. The OU process is defined by the stochastic differential equation (SDE):

$$d\mathbf{x}_t = -\frac{1}{2}\mathbf{x}_t dt + d\mathbf{W}_t, \quad (18)$$

in which t is the forward time of the diffusion process, \mathbf{x}_t is the noise contaminated image at time t , and \mathbf{W}_t is a standard Brownian motion. The standard Brownian motion formally satisfies $d\mathbf{W}_t = \sqrt{dt}\epsilon$ with ϵ be a standard Gaussian noise. In practice, the OU process is numerically discretized into the variance-preserving (VP) form (Song et al., 2020b):

$$\mathbf{x}_i = \sqrt{1 - \beta_{i-1}}\mathbf{x}_{i-1} + \sqrt{\beta_{i-1}}\epsilon_{i-1}, \quad (19)$$

where $i = 1, \dots, n$ is the number of the time step, β_i is the step size of each time step, \mathbf{x}_i is image at i th time step with time $t_i = \sum_{j=0}^{i-1} \beta_j$, ϵ_i is standard Gaussian random variable. The time step size usually takes the form $\beta_i = \frac{i(b_2 - b_1)}{n-1} + b_1$ where $b_1 = 10^{-4}$ and $b_2 = 0.02$. Note that our interpretation of β differs from that in (Song et al., 2020b), treating β as a varying time-step size to solve the autonomous SDE (18) instead of a time-dependent SDE. Our interpretation holds as long as every β_i^2 is negligible and greatly simplifies future analysis. The discretized OU process (19) adds a small amount of Gaussian noise to the image at each time step i , gradually contaminating the image until $\mathbf{x}_n \sim \mathcal{N}(\mathbf{0}, I)$.

Training a DDPM aims to recover the original image \mathbf{x}_0 from one of its contaminated versions \mathbf{x}_i . In this case (19) could be rewritten into the form

$$\mathbf{x}_i = \sqrt{\bar{\alpha}_i}\mathbf{x}_0 + \sqrt{1 - \bar{\alpha}_i}\bar{\epsilon}_i; \quad 1 \leq i \leq n, \quad (20)$$

where $\bar{\alpha}_i = \prod_{j=0}^{i-1} (1 - \beta_j)$ is the weight of contamination and $\bar{\epsilon}_i$ is a standard Gaussian random noise to be removed. This equation tells us that the distribution of \mathbf{x}_i given \mathbf{x}_0 is a Gaussian distribution

$$p(\mathbf{x}_i|\mathbf{x}_0) = \mathcal{N}(\mathbf{x}|\sqrt{\bar{\alpha}_i}\mathbf{x}_0, (1 - \bar{\alpha}_i)I), \quad (21)$$

and the noise $\bar{\epsilon}_i$ is related to the its score function

$$\bar{\epsilon}_i = -\sqrt{1 - \bar{\alpha}_i}\mathbf{s}(\mathbf{x}_i|\mathbf{x}_0, t_i), \quad (22)$$

where $\mathbf{s}(\mathbf{x}_i|\mathbf{x}_0, t_i) = \nabla_{\mathbf{x}_i} \log p(\mathbf{x}_i|\mathbf{x}_0)$ is the score of the density $p(\mathbf{x}_i|\mathbf{x}_0)$ at \mathbf{x}_i .

DDPM aims to removes the noise $\bar{\epsilon}_i$ from \mathbf{x}_i by training a denoising neural network $\epsilon_\theta(\mathbf{x}, t_i)$ to predict and remove the noise $\bar{\epsilon}_i$. This means that DDPM minimizes the denoising objective (Ho et al., 2020):

$$L_{denoise}(\epsilon_\theta) = \frac{1}{n} \sum_{i=1}^n \mathbf{E}_{\mathbf{x}_0 \sim p(\mathbf{x})} \mathbf{E}_{\bar{\epsilon}_i \sim \mathcal{N}(\mathbf{0}, I)} \|\bar{\epsilon}_i - \epsilon_\theta(\mathbf{x}_i, t_i)\|_2^2. \quad (23)$$

This is equivalent to, with the help of (22) and tricks in (Vincent, 2011), a denoising score matching objective

$$L_{denoise}(\epsilon_\theta) = \frac{1}{n} \sum_{i=1}^n (1 - \bar{\alpha}_i) \mathbf{E}_{\mathbf{x}_i \sim p(\mathbf{x}_i)} \left\| \mathbf{s}(\mathbf{x}_i, t_i) + \frac{\epsilon_\theta(\mathbf{x}_i, t_i)}{\sqrt{1 - \bar{\alpha}_i}} \right\|_2^2. \quad (24)$$

where $\mathbf{s}(\mathbf{x}, t_i) = \nabla_{\mathbf{x}_i} \log p(\mathbf{x}_i)|_{\mathbf{x}_i=\mathbf{x}}$ is the score function of the density $p(\mathbf{x}_i)$. This objectives says that the denoising neural network $\epsilon_\theta(\mathbf{x}, t_i)$ is trained to approximate a scaled score function $\epsilon(\mathbf{x}, t_i)$ (Yang et al., 2022)

$$\epsilon(\mathbf{x}, t_i) = \underset{\epsilon_\theta}{\operatorname{argmin}} L(\epsilon_\theta) = -\sqrt{1 - \bar{\alpha}_i}\mathbf{s}(\mathbf{x}, t_i). \quad (25)$$

Another useful property we shall exploit later is that for **infinitesimal** time steps, the contamination weight $\bar{\alpha}_i$ is the exponential of the diffusion time t_i

$$\lim_{\max_j \beta_j \rightarrow 0} \bar{\alpha}_i \rightarrow e^{-t_i}. \quad (26)$$

In this case, the discretized OU process (19) is equivalent to the OU process (18), hence the scaled score function $\epsilon(\mathbf{x}, t_i)$ is

$$\epsilon(\mathbf{x}, t) = -\sqrt{1 - e^{-t}}\mathbf{s}(\mathbf{x}, t), \quad (27)$$

where $\mathbf{s}(\mathbf{x}, t)$ is a solution of the score Fokker-Planck equation (37) of the OU process.

The backward diffusion process is used to sample from the DDPM by removing the noise of an image step by step. It is the time reversed version of the OU process, starting at $x_{0'} \sim \mathcal{N}(\mathbf{x}|\mathbf{0}, I)$, using the reverse of the OU process (Anderson, 1982):

$$d\mathbf{x}_{t'} = \left(\frac{1}{2}\mathbf{x}_{t'} + \mathbf{s}(\mathbf{x}, T - t') \right) dt' + d\mathbf{W}_{t'}, \quad (28)$$

in which $t' \in [0, T]$ is the backward time, $\mathbf{s}(\mathbf{x}, T - t') = \nabla_{\mathbf{x}_{T-t'}} \log p(\mathbf{x}_{T-t'})|_{\mathbf{x}}$ is the score function of the density of $\mathbf{x}_{t=T-t'}$ in the forward process. In practice, the backward diffusion process is discretized into

$$\mathbf{x}_{i'+1} = \frac{\mathbf{x}_{i'} + \mathbf{s}(\mathbf{x}_{i'}, T - t_{i'})\beta_{n-i'}}{\sqrt{1 - \beta_{n-i'}}} + \sqrt{\beta_{n-i'}}\boldsymbol{\epsilon}_{i'}, \quad (29)$$

where $i' = 0, \dots, n$ is the number of the backward time step, $\mathbf{x}_{i'}$ is image at i' th backward time step with time $t_{i'} = \sum_{j=0}^{i'-1} \beta_{n-1-j} = T - t_{n-i'}$, and $\mathbf{s}(\mathbf{x}_{i'}, T - t_{i'})$ is estimated by (25). This discretization is consistent with (28) as long as β_i^2 are negligible.

The forward and backward process forms a dual pair when total diffusion time t_n is large enough and the time step sizes are small enough, at which $p(\mathbf{x}_n) = \mathcal{N}(\mathbf{0}, I)$. In this case the density of \mathbf{x}_t in the forward process and the density of $\mathbf{x}_{t'}$ in the backward process satisfying the relation

$$p(\mathbf{x}_{t'})|_{t'=T-t} = p(\mathbf{x}_t). \quad (30)$$

This relation tells us that the discrete backward diffusion process generate image samples approximately from the image distribution

$$p(\mathbf{x}_{n'}) \approx p(\mathbf{x}_0) = p(\mathbf{x}), \quad (31)$$

despite the discretization error and estimation error of the score function $\mathbf{s}(\mathbf{x}, t')$. An accurate estimation of the score function is one of the key to sample high quality images.

B. Conditional DDPM and Guidance

Conditional DDPMs, which generate images based on a given condition \mathbf{c} , model the conditional image distribution $p(\mathbf{x}|\mathbf{c})$. One can introduce the dependency on conditions by extending the denoising neural network to include the condition \mathbf{c} , represented as $\epsilon(\mathbf{x}|\mathbf{c}, t_i)$.

Guidance is a technique for conditional image generation that trades off control strength and image diversity. It aims to sample from the distribution (Song et al., 2020b; Dhariwal & Nichol, 2021)

$$p(\mathbf{x}|\mathbf{c}, \omega) \propto p(\mathbf{c}|\mathbf{x})^{1+\omega} p(\mathbf{x}), \quad (32)$$

where $\omega > 0$ is the guidance scale. When ω is large, guidance control the DDPM to produce samples that have the highest classifier likelihood $p(\mathbf{c}|\mathbf{x})$.

Another equivalent guidance without the need of the classifier $p(\mathbf{c}|\mathbf{x})$ is the Classifier-free guidance (Ho, 2022):

$$p(\mathbf{x}|\mathbf{c}, \omega) \propto p(\mathbf{x}|\mathbf{c})^{1+\omega} p(\mathbf{x})^{-\omega}, \quad (33)$$

Sampling from $p(\mathbf{x}|\mathbf{c}, \omega)$ using DDPM requires the corresponding denoising neural network $\epsilon(\mathbf{x}|\mathbf{c}, t_i, \omega)$ that is unknown. Classifier-free guidance provides an approximation of it by linearly combine $\epsilon(\mathbf{x}|\mathbf{c}, t_i)$ and $\epsilon(\mathbf{x}, t_i)$ of conditional and

unconditional DDPMs. The classifier-free guidance is inspired by the fact that ϵ is proportional to the score \mathbf{s} in (25). At $t = t_0 = 0$, the score of the distribution $p(\mathbf{x}|\mathbf{c}, \omega)$ is the linear combination of scores of $p(\mathbf{x}|\mathbf{c})$ and $p(\mathbf{x})$:

$$\mathbf{s}(\mathbf{x}|\mathbf{c}, t_0, \omega) = (1 + \omega) \mathbf{s}(\mathbf{x}|\mathbf{c}, t_0) - \omega \mathbf{s}(\mathbf{x}, t_0), \quad (34)$$

where $\mathbf{s}(\mathbf{x}|\mathbf{c}, t_0, \omega) = \nabla_{\mathbf{x}} \log p(\mathbf{x}|\mathbf{c}, \omega)$, $\mathbf{s}(\mathbf{x}|\mathbf{c}, t_0) = \nabla_{\mathbf{x}} \log p(\mathbf{x}|\mathbf{c})$, and $\mathbf{s}(\mathbf{x}, t_0) = \nabla_{\mathbf{x}} \log p(\mathbf{x})$. Since scores \mathbf{s} are proportional to de-noising neural networks ϵ according to equation (25), equation (34) inspires the classifier free guidance to use the following guided denoising neural network $\epsilon_{CF}(\mathbf{x}|\mathbf{c}, t_i, \omega)$:

$$\epsilon_{CF}(\mathbf{x}|\mathbf{c}, t_i, \omega) = (1 + \omega) \epsilon_{\theta}(\mathbf{x}|\mathbf{c}, t_i) - \omega \epsilon_{\theta}(\mathbf{x}, t_i), \quad (35)$$

where i is the number of time step, $t_i = \sum_{j=0}^i \beta_j$, \mathbf{c} is the condition, and $\omega > 0$ is the guidance scale. The classifier free guidance exactly computes the de-noising neural network $\epsilon(\mathbf{x}|\mathbf{c}, t_i, \omega)$ of $p(\mathbf{x}|\mathbf{c}, \omega)$ at time $t_0 = 0$ because of the connection between score function and ϵ (25). However, ϵ_{CF} is not a good approximation of the theoretical $\epsilon(\mathbf{x}|\mathbf{c}, t_i, \omega)$ for most of time steps $0 < i < n$ when the guidance scale ω is large.

C. Fokker-Planck Equation

The probability density distribution $p(\mathbf{x}_t)$ of the diffusion process (18) is a function of \mathbf{x} and t , governed by the Fokker-Planck equation of the OU process:

$$\frac{\partial p}{\partial t} = \frac{1}{2} \nabla_{\mathbf{x}} \cdot (\mathbf{x}p) + \frac{1}{2} \nabla_{\mathbf{x}}^2 p. \quad (36)$$

The corresponding score function $\mathbf{s} = \nabla_{\mathbf{x}} \log p$ is a vector valued function of \mathbf{x} and t governed by the score Fokker-Planck equation:

$$\frac{\partial \mathbf{s}}{\partial t} = \frac{1}{2} (\nabla_{\mathbf{x}}(\mathbf{s} \cdot \mathbf{x}) + \nabla_{\mathbf{x}}^2 \mathbf{s} + \nabla_{\mathbf{x}} \|\mathbf{s}\|_2^2) \quad (37)$$

that has been recently studied by (Lai et al., 2022) (our score Fokker-Planck equation differs from theirs slightly by noting that $\nabla_{\mathbf{x}} \nabla_{\mathbf{x}} \cdot \mathbf{s} = \nabla_{\mathbf{x}}^2 \mathbf{s}$ where \mathbf{s} is a gradient). This equation holds for both unconditional, conditional, and guided DDPM because they share the same forward diffusion process. Their corresponding initial conditions at time $t = t_0 = 0$ are $\mathbf{s}(\mathbf{x}, t_0)$, $\mathbf{s}(\mathbf{x}|\mathbf{c}, t_0)$ and $\mathbf{s}(\mathbf{x}|\mathbf{c}, t_0, \omega)$.

However, the score Fokker-Planck equation is a non-linear partial differential equation, which means a linear combination of scores of the unconditional and conditional DDPM is not equivalent to the guided score:

$$\mathbf{s}(\mathbf{x}|\mathbf{c}, t, \omega) \neq (1 + \omega) \mathbf{s}(\mathbf{x}|\mathbf{c}, t) - \omega \mathbf{s}(\mathbf{x}, t); \quad t_0 < t < t_n, \quad (38)$$

even though their initial conditions at $t = t_0 = 0$ satisfies the linear relation (34). Consequently, the classifier-free guidance ϵ_{CF} is not a good approximation of ϵ for $p(\mathbf{x}|\mathbf{c}, \omega)$ at $t_0 < t < t_n$. Furthermore, ϵ_{CF} does not correspond to a DDPM of any distribution $p(\mathbf{x})$ when $\omega > 0$, because all DDPMs theoretically have corresponding scores satisfying the score Fokker-Planck (37) while ϵ_{CF} does not.

Our work aims to address this issue by providing non-linear corrections to the classifier-free guidance, making it approximately satisfy the score Fokker-Planck equation. We propose the Harmonic ansatz which says the Laplacian term $\nabla_{\mathbf{x}}^2 \mathbf{s}$ in the score Fokker-Planck equation is negligible. It allow us to use the method of characteristics to handle the non-linear term. Noting from (25) that $\epsilon \propto -\mathbf{s}$, the Harmonic ansatz stands as a good approximation as long as $\|\nabla_{\mathbf{x}}^2 \epsilon\| \ll \|-\nabla_{\mathbf{x}}(\epsilon \cdot \mathbf{x}) + \nabla_{\mathbf{x}} \|\epsilon\|_2^2\|$ along possible diffusion trajectories of DDPM.

D. Fixed Point Iteration Methods for Solving the Correction Term

We solve $\Delta \mathbf{x}$ from the equation (7) by fixed point iterative methods. The key idea is treating the residual vector \mathbf{g} of the equation (7)

$$\mathbf{g} = \Delta \mathbf{x} - \mathbf{P} \circ (\epsilon_{\theta}(\mathbf{x}_2, t_i) - \epsilon_{\theta}(\mathbf{x}_1|\mathbf{c}, t_i)) \sigma_i,$$

as the gradient in an optimization problem. Consequently we could apply any off-the-shelf optimization algorithm to solve the fixed point iteration problem.

For example, adopting the gradient descent methods in leads us to the well-known successive over-relaxation iteration method for fixed point problem (Alg.1). Similarly, adopting the RMSprop method leads us to Alg.2 with faster convergence.

Algorithm 1 Successive over-relaxation iteration for $\Delta \mathbf{x}$

Require: $\mathbf{x}, \mathbf{c}, t_i, \omega, \epsilon_\theta, \sigma_i, \bar{\alpha}_i, \eta$ (tolerance), γ (relaxation factor)

Require: $\mathbf{x}, \mathbf{c}, t_i, \omega, \sigma_i$ {Inputs for the DDPM model}

Require: γ (lr) {Standard parameters for gradient descent}

Require: η {The tolerance as stopping criteria}

Ensure: $\Delta \mathbf{x}$

- 1: Initialize $\Delta \mathbf{x}^{(0)}$ as a zero vector
 - 2: Set $k = 0$
 - 3: **repeat**
 - 4: $k \leftarrow k + 1$
 - 5: $\mathbf{x}_1^{(k-1)} = \mathbf{x} + \omega \Delta \mathbf{x}^{(k-1)}$
 - 6: $\mathbf{x}_2^{(k-1)} = \mathbf{x} + (1 + \omega) \Delta \mathbf{x}^{(k-1)}$
 - 7: $\mathbf{g}^{(k)} = \Delta \mathbf{x}^{(k-1)} - \mathbf{P} \circ \left(\epsilon_\theta(\mathbf{x}_2^{(k-1)}, t_i) - \epsilon_\theta(\mathbf{x}_1^{(k-1)} | \mathbf{c}, t_i) \right) \sigma_i$,
 - 8: Update $\Delta \mathbf{x}^{(k)} = \Delta \mathbf{x}^{(k-1)} - \gamma \mathbf{g}^{(k)}$,
 - 9: **until** $\|\mathbf{g}\|_2^2 < \eta^2 \dim(\mathbf{g})$
 - 10: Return $\Delta \mathbf{x}^{(k)}$ as $\Delta \mathbf{x}$
-

Algorithm 2 RMSprop iteration for $\Delta \mathbf{x}$

Require: $\mathbf{x}, \mathbf{c}, t_i, \omega, \sigma_i$ {Inputs for the DDPM model}

Require: α, ϵ, γ (lr) {Standard parameters for the RMSprop algorithm}

Require: η {The tolerance as stopping criteria}

Require: D {Learning rate schedule}

Ensure: $\Delta \mathbf{x}$

- 1: Initialize $\Delta \mathbf{x}^{(0)}$ as a zero vector
 - 2: Set $k = 0$
 - 3: **repeat**
 - 4: $k \leftarrow k + 1$
 - 5: $\mathbf{x}_1^{(k-1)} = \mathbf{x} + \omega \Delta \mathbf{x}^{(k-1)}$
 - 6: $\mathbf{x}_2^{(k-1)} = \mathbf{x} + (1 + \omega) \Delta \mathbf{x}^{(k-1)}$
 - 7: $\mathbf{g}^{(k)} = \Delta \mathbf{x}^{(k-1)} - \mathbf{P} \circ \left(\epsilon_\theta(\mathbf{x}_2^{(k-1)}, t_i) - \epsilon_\theta(\mathbf{x}_1^{(k-1)} | \mathbf{c}, t_i) \right) \sigma_i$,
 - 8: $\mathbf{v}^{(k)} = \alpha \mathbf{v}^{(k-1)} + (1 - \alpha) (\mathbf{g}^{(k)})^2$
 - 9: $\gamma^{(k)} = \gamma / (1 + Dk)$
 - 10: Update $\Delta \mathbf{x}^{(k)} = \Delta \mathbf{x}^{(k-1)} - \gamma^{(k)} \mathbf{g}^{(k)} / (\sqrt{\mathbf{v}^{(k)}} + \epsilon)$,
 - 11: **until** $\|\mathbf{g}\|_2^2 < \eta^2 \dim(\mathbf{g})$
 - 12: Return $\Delta \mathbf{x}^{(k)}$ as $\Delta \mathbf{x}$
-

Another kind of effective iteration method to solve $\Delta \mathbf{x}$ is the Anderson acceleration method (Walker & Ni, 2011) Alg.3, which turns out to be faster than RMSprop when applied to latent diffusion models.

Algorithm 3 Anderson acceleration (AA) iteration for $\Delta \mathbf{x}$

Require: $\mathbf{x}, \mathbf{c}, t_i, \omega, \sigma_i$ {Inputs for the DDPM model}
Require: $m \geq 2, \gamma$ (lr), $\Delta \mathbf{x}_B = []$, $\mathbf{g}_B = []$ {Parameters and buffers for AA algorithm}
Require: η {The tolerance as stopping criteria}
Ensure: $\Delta \mathbf{x}$

- 1: Initialize $\Delta \mathbf{x}^{(0)}$ as a zero vector
- 2: Set $k = 0$
- 3: **repeat**
- 4: $k \leftarrow k + 1$
- 5: $\mathbf{x}_1^{(k-1)} = \mathbf{x} + \omega \Delta \mathbf{x}^{(k-1)}$
- 6: $\mathbf{x}_2^{(k-1)} = \mathbf{x} + (1 + \omega) \Delta \mathbf{x}^{(k-1)}$
- 7: $\mathbf{g}^{(k)} = \Delta \mathbf{x}^{(k-1)} - \mathbf{P} \circ \left(\epsilon_\theta(\mathbf{x}_2^{(k-1)}, t_i) - \epsilon_\theta(\mathbf{x}_1^{(k-1)} | \mathbf{c}, t_i) \right) \sigma_i$,
- 8: $\Delta \mathbf{x}_B.append(\Delta \mathbf{x}^{(k-1)})$, $\mathbf{g}_B.append(\mathbf{g}^{(k)})$
- 9: **if** $\text{len}(\Delta \mathbf{x}_B) \geq 2$ **then**
- 10: $\mathbf{g}_B[-2] = \mathbf{g}_B[-1] - \mathbf{g}_B[-2]$
- 11: $\Delta \mathbf{x}_B[-2] = \Delta \mathbf{x}_B[-1] - \Delta \mathbf{x}_B[-2]$
- 12: **if** $\text{len}(\Delta \mathbf{x}_B) > m$ **then**
- 13: $\text{del } \mathbf{g}_B[0]$; $\text{del } \Delta \mathbf{x}_B[0]$;
- 14: **end if**
- 15: $A_g = \mathbf{g}_B[: -1]$; $A_x = \Delta \mathbf{x}_B[: -1]$;
- 16: $\mathbf{b}_g = \mathbf{g}_B[-1]$; $\mathbf{b}_x = \Delta \mathbf{x}_B[-1]$;
- 17: $\mathbf{w} = \text{argmin}_{\mathbf{w}} \|A_g \mathbf{w} - \mathbf{b}_g\|_2^2$
- 18: $\Delta \mathbf{x}_{AA}^{(k-1)} = \mathbf{b}_x - A_x \mathbf{w}$
- 19: $\mathbf{g}_{AA}^{(k)} = \mathbf{b}_g - A_g \mathbf{w}$
- 20: **else**
- 21: $\Delta \mathbf{x}_{AA}^{(k-1)} = \Delta \mathbf{x}^{(k-1)}$
- 22: $\mathbf{g}_{AA}^{(k)} = \mathbf{g}^{(k)}$
- 23: **end if**
- 24: Update $\Delta \mathbf{x}^{(k)} = \Delta \mathbf{x}_{AA}^{(k-1)} - \gamma \mathbf{g}_{AA}^{(k)}$,
- 25: **until** $\|\mathbf{g}\|_2^2 < \eta^2 \text{dim}(\mathbf{g})$
- 26: Return $\Delta \mathbf{x}^{(k)}$ as $\Delta \mathbf{x}$

In practice, the number of iterations required to solve $\Delta \mathbf{x}$ depends on both the iteration method and the DDPM model. Different iteration methods may have different convergence rates and stability properties. Therefore, we suggest trying different iteration methods to find the most efficient and effective one for a given DDPM model.

E. Deriving the Characteristic Guidance Using the Method of Characteristics

The exactness of the classifier-free guidance revealed by (34) as initial condition at $t_0 = 0$ and its failure at $t_i > t_0$ due to non-linearity (38) are key observations that inspires the characteristic guidance. Characteristic guidance answers the following problem: Given two known solutions $\mathbf{s}_1(\mathbf{x}, t)$ and $\mathbf{s}_2(\mathbf{x}, t)$ of the score Fokker-Planck equation (37), compute another solution $\mathbf{s}(\mathbf{x}, t)$ of the score Fokker-Planck equation with the following initial condition:

$$\mathbf{s}(\mathbf{x}, 0) = (1 + \omega)\mathbf{s}_1(\mathbf{x}, 0) - \omega\mathbf{s}_2(\mathbf{x}, 0), \quad (39)$$

Note that this initial condition is the same as the condition $\epsilon(\mathbf{x}, 0) = (1 + \omega)\epsilon_1(\mathbf{x}, 0) - \omega\epsilon_2(\mathbf{x}, 0)$ used in lemma 4.2 because score \mathbf{s} is proportional to ϵ (25). Similarly, the problem is equivalent to express $\epsilon(\mathbf{x}, t)$ in terms of $\epsilon_1(\mathbf{x}, t)$ and $\epsilon_2(\mathbf{x}, t)$ as stated in lemma 4.2.

It is not easy to express $\mathbf{s}(\mathbf{x}, t)$ as a function of $\mathbf{s}_1(\mathbf{x}, t)$ and $\mathbf{s}_2(\mathbf{x}, t)$ without training or taking complex derivatives. Fortunately, the harmonic ansatz 4.1 leads us to a viable solution. **The harmonic ansatz** reduces the score Fokker-Planck

equation (37) to the following non-linear first-order partial differential equation (PDE)

$$\frac{\partial \mathbf{s}}{\partial t} = \frac{1}{2} (\nabla_{\mathbf{x}}(\mathbf{s} \cdot \mathbf{x}) + \nabla_{\mathbf{x}} \|\mathbf{s}\|_2^2), \quad (40)$$

where the Laplacian term is omitted but the non-linear term remains, capturing the non-linear effect in DDPMs. We treat $\mathbf{s}(\mathbf{x}, t)$, $\mathbf{s}_1(\mathbf{x}, t)$, and $\mathbf{s}_2(\mathbf{x}, t)$ as solutions to this PDE and deduce $\mathbf{s}(\mathbf{x}, t)$ using the method of characteristics.

Characteristic Lines The method of characteristics reduce a partial differential equation to a family of ordinary differential equations (ODE) by considering solutions along characteristic lines. In our case, we consider the characteristic lines $\mathbf{x}(t)$ satisfying the ODE:

$$\frac{d\mathbf{x}(t)}{dt} = - \left(\frac{1}{2} \mathbf{x} + \mathbf{s}(\mathbf{x}(t), t) \right), \quad (41)$$

substitute such characteristic lines into the PDE (40) yields the dynamics of the score functions along the lines

$$\frac{d\mathbf{s}(\mathbf{x}(t), t)}{dt} = \frac{1}{2} \mathbf{s}(\mathbf{x}(t), t), \quad (42)$$

The characteristic lines of the simplified score Fokker-Planck equation (40), which are solutions of the ODEs (41) and (42), has the form

$$\begin{aligned} \mathbf{x}(t) &= e^{-\frac{t}{2}} \mathbf{x}_0 - (1 - e^{-t}) \mathbf{s}(\mathbf{x}(t), t) \\ \mathbf{s}(\mathbf{x}(t), t) &= \mathbf{s}(\mathbf{x}_0, 0) e^{\frac{t}{2}}, \end{aligned} \quad (43)$$

where $\mathbf{x}_0 = \mathbf{x}(0)$ is the starting point of the line and serves as a constant parameter, $\mathbf{s}(\mathbf{x}_0, 0)$ depends on the initial condition of \mathbf{s} at $t = 0$. An important remark on the characteristic lines is that (43) is valid for \mathbf{s}_1 and \mathbf{s}_2 as well, if we replace every \mathbf{s} with \mathbf{s}_1 or \mathbf{s}_2 . This is because \mathbf{s} , \mathbf{s}_1 , and \mathbf{s}_2 are solutions to the same PDE (40). The merit of these characteristic lines lies in their ability to determine the value of $\mathbf{s}(\mathbf{x}(t), t)$ at $t > 0$ using information of \mathbf{x}_0 and $\mathbf{s}(\mathbf{x}_0, 0)$ at $t = 0$, thereby allowing us to utilize the initial condition (39).

Deducing $\mathbf{s}(\mathbf{x}, t)$ Our next move is deduce the value $\mathbf{s}(\mathbf{x}, t)$ from $\mathbf{s}_1(\mathbf{x}, t)$ and $\mathbf{s}_2(\mathbf{x}, t)$ with the help of characteristic lines. Denote the characteristic lines of the three score functions \mathbf{s} , \mathbf{s}_1 , and \mathbf{s}_2 to be $\mathbf{x}(t)$, $\mathbf{x}_1(t)$, $\mathbf{x}_2(t)$. If the three characteristic lines meets at \mathbf{x}_0 at $t = 0$

$$\mathbf{x}(0) = \mathbf{x}_1(0) = \mathbf{x}_2(0) = \mathbf{x}_0, \quad (44)$$

then the initial condition (39) and the equation (43) tells that

$$\mathbf{s}(\mathbf{x}(t), t) = (1 + \omega) \mathbf{s}_1(\mathbf{x}_1(t), t) - \omega \mathbf{s}_2(\mathbf{x}_2(t), t), \quad (45)$$

which achieves our goal in expressing the value \mathbf{s} in terms of \mathbf{s}_1 and \mathbf{s}_2 . In summary, the following system of equations determines the value of \mathbf{s} in terms of \mathbf{s}_1 and \mathbf{s}_2

$$\begin{cases} \mathbf{x}(t) e^{\frac{t}{2}} + (e^{\frac{t}{2}} - e^{-\frac{t}{2}}) \mathbf{s}(\mathbf{x}(t), t) &= \mathbf{x}_0 \\ \mathbf{x}_1(t) e^{\frac{t}{2}} + (e^{\frac{t}{2}} - e^{-\frac{t}{2}}) \mathbf{s}_1(\mathbf{x}_1(t), t) &= \mathbf{x}_0 \\ \mathbf{x}_2(t) e^{\frac{t}{2}} + (e^{\frac{t}{2}} - e^{-\frac{t}{2}}) \mathbf{s}_2(\mathbf{x}_2(t), t) &= \mathbf{x}_0 \\ (1 + \omega) \mathbf{s}_1(\mathbf{x}_1(t), t) - \omega \mathbf{s}_2(\mathbf{x}_2(t), t) &= \mathbf{s}(\mathbf{x}(t), t), \end{cases} \quad (46)$$

in which the first three equations are reformulations of (43) and say that the three characteristic lines meets at the same \mathbf{x}_0 at $t = 0$. In practice, we wish to compute the value of \mathbf{s} for a given $\mathbf{x}(t)$ at time t , with the functions \mathbf{s}_1 and \mathbf{s}_2 known in advance. This completes the system with four equations and four unknowns: \mathbf{x}_0 , $\mathbf{x}_1(t)$, $\mathbf{x}_2(t)$, and $\mathbf{s}(\mathbf{x}(t), t)$.

Since the dependency of \mathbf{x} on t is already characterized by the system of equation, we can simplify the notation by omitting it in the following discussion. Hence, we write \mathbf{x} , \mathbf{x}_1 , \mathbf{x}_2 instead of $\mathbf{x}(t)$, $\mathbf{x}_1(t)$, $\mathbf{x}_2(t)$ in the following discussion.

Simplify the System It is possible to simplify the system of four equations into one. We start from eliminating the unknowns $\mathbf{s}(\mathbf{x}, t)$ and \mathbf{x}_0 with some algebra, reducing the system into two equations

$$\begin{cases} \mathbf{x}_1 &= \mathbf{x} + \omega (\mathbf{s}_1(\mathbf{x}_1, t) - \mathbf{s}_2(\mathbf{x}_2, t)) (1 - e^{-t}) \\ \mathbf{x}_2 &= \mathbf{x} + (1 + \omega) (\mathbf{s}_1(\mathbf{x}_1, t) - \mathbf{s}_2(\mathbf{x}_2, t)) (1 - e^{-t}). \end{cases} \quad (47)$$

The above equations also indicate that \mathbf{x}_1 and \mathbf{x}_2 are not independent but linearly correlated as

$$(1 + \omega)\mathbf{x}_1 - \omega\mathbf{x}_2 = \mathbf{x}. \quad (48)$$

This inspires us to define the correction term $\Delta\mathbf{x}$ as

$$\begin{aligned} \mathbf{x}_1 &= \mathbf{x} + \omega\Delta\mathbf{x} \\ \mathbf{x}_2 &= \mathbf{x} + (1 + \omega)\Delta\mathbf{x}, \end{aligned} \quad (49)$$

which is exactly the same notation used in the characteristic guidance (6).

Finally, by combining (47) and (48), we obtain a single equation for $\Delta\mathbf{x}$ as follows:

$$\Delta\mathbf{x} = (\mathbf{s}_1(\mathbf{x} + \omega\Delta\mathbf{x}, t) - \mathbf{s}_2(\mathbf{x} + (1 + \omega)\Delta\mathbf{x}, t)) (1 - e^{-t}). \quad (50)$$

Once we solve for $\Delta\mathbf{x}$ from the above equation, we can easily compute the desired value of the score function $\mathbf{s}(\mathbf{x}, t)$ by using (49) and (46):

$$\mathbf{s}(\mathbf{x}, t) = (1 + \omega)\mathbf{s}_1(\mathbf{x}_1, t) - \omega\mathbf{s}_2(\mathbf{x}_2, t). \quad (51)$$

Characteristic Guidance and Lemma 4.2 Now we have nearly completed the derivation of the characteristic guidance. It remains to replace the score functions \mathbf{s} with the de-noising neural networks ϵ used in DDPM. They are related by (27) if the diffusion time steps in DDPM are small enough. Consequently we rewrite (51) and (50) into

$$\epsilon(\mathbf{x}, t) = (1 + \omega)\epsilon_1(\mathbf{x}_1, t) - \omega\epsilon_2(\mathbf{x}_2, t), \quad (52)$$

and

$$\Delta\mathbf{x} = (\epsilon_2(\mathbf{x}_2, t) - \epsilon_1(\mathbf{x}_1, t)) \sigma(t), \quad (53)$$

where $\sigma(t) = \sqrt{1 - e^{-t}}$. These equations are exactly the content of the Lemma 4.2.

In practice, DDPMs do not use infinitesimal time steps. Therefore we replace e^{-t_i} with $\bar{\alpha}_i$ everywhere since they are related through (26). This leads to the characteristic guidance (6) and (7).

F. Conditional Gaussian

This experiment compares the classifier free guidance and the characteristic guidance on sampling from a conditional 2D Gaussian distributions, which strictly satisfies the harmonic ansatz.

The diffusion model models two distribution: the conditional distribution $p(x_1, x_2 | c_1, c_2)$ and the unconditional distribution $p(x_1, x_2)$. In our case, both of them are 2D Gaussian distributions

$$\begin{aligned} p(x_1, x_2 | c_1, c_2) &= \mathcal{N}(x_1, x_2 | (c_1, c_2)^T, I) \\ p(x_1, x_2) &= \mathcal{N}(x_1, x_2 | (0, 0)^T, 5I) \end{aligned} \quad (54)$$

The guided diffusion model (33) aims to sample from the distribution

$$p(x_1, x_2 | c_1, c_2; \omega) = \mathcal{N}\left(x_1, x_2 | \left(\frac{5c_1(\omega + 1)}{4\omega + 5}, \frac{5c_2(\omega + 1)}{4\omega + 5}\right)^T, \frac{5}{4\omega + 5}I\right) \quad (55)$$

having the properties $p(x_1, x_2 | c_1, c_2; 0) = p(x_1, x_2 | c_1, c_2)$ and $p(x_1, x_2 | c_1, c_2; -1) = p(x_1, x_2)$.

The score function of the unconditional, conditional, and guided model along the forward diffusion process can be solved analytically from the Fokker-Planck equation:

$$\mathbf{s}(x_1, x_2 | c_1, c_2; t, \omega) = \left(\frac{5c_1(\omega + 1)e^{t/2} - (4\omega + 5)e^t x_1}{(4\omega + 5)e^t - 4\omega}, \frac{5c_2(\omega + 1)e^{t/2} - (4\omega + 5)e^t x_2}{(4\omega + 5)e^t - 4\omega} \right)^T$$

with $\omega = -1$ and $\omega = 0$ corresponds to the scores of unconditional and conditional distributions. Therefore the denoising neural networks ϵ_θ of unconditional and conditional DDPMs could be analytically calculated as

$$\begin{aligned}\epsilon_\theta(x_1, x_2, t) &= -\sqrt{1 - e^{-t}}\mathbf{s}(x_1, x_2; t, -1) \\ \epsilon_\theta(x_1, x_2|c_1, c_2; t) &= -\sqrt{1 - e^{-t}}\mathbf{s}(x_1, x_2|c_1, c_2; t, 0)\end{aligned}\quad (56)$$

The corresponding classifier free guided ϵ_{CF} and characteristic guided ϵ_{CH} are computed according to (35) and (6). The characteristic guidance is computed with Alg.2 with $\gamma = 0.01$, $\eta = 0.01$, and $\alpha = 0.9999$.

We sample from guided DDPMs using four different ways: the SDE (29), probabilistic ODE (Song et al., 2020b), DDIM (Song et al., 2020a), and DPM++2M (Lu et al., 2022). We set $c_1 = -5$, $c_2 = 5$, $\beta_1 = 1e - 4$, $\beta_2 = 0.015$ and the total time step to be $n = 1000$ for SDE and ODE, and $n = 20$ for DDIM and DPM++2M. The sample results are compared with the theoretical reference distribution (55) by assuming the samples are Gaussian distributed then computing the KL divergence with the theoretical reference. The results are plotted in Fig.9. Our characteristic guidance outperforms classifier free guidance in all cases with $\omega > 0$.

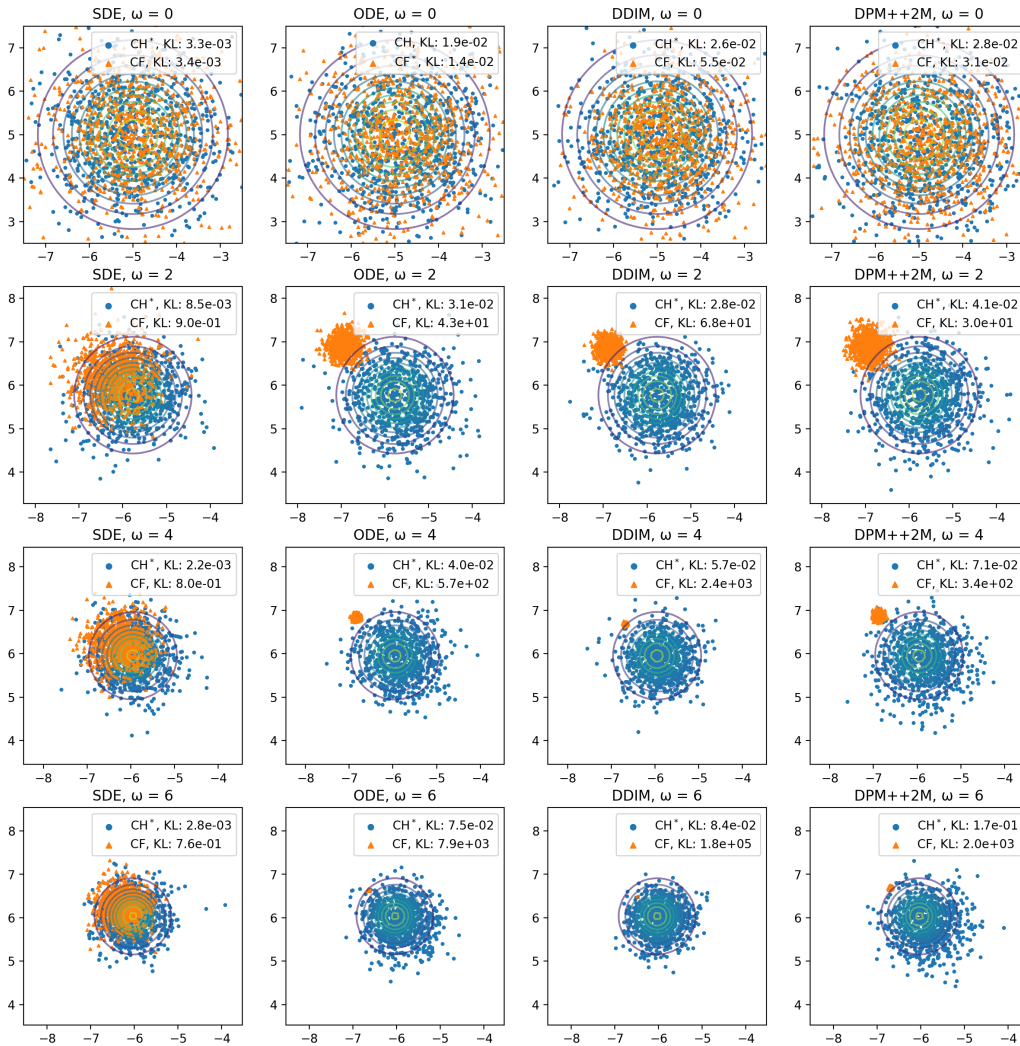


Figure 9. Comparison between characteristic guidance (CH) and classifier free guidance (CF) of DDPM on the conditional Gaussian experiment. Samples are drawn with various sample methods: SDE, probabilistic ODE, DDIM and DPM++2M. The contours corresponds to the theoretical reference distribution of guided DDPMs in (55).

G. Mixture of Gaussian

This experiment compares the classifier free guidance and the characteristic guidance when the assumption $\nabla_{\mathbf{x}} \nabla_{\mathbf{x}} \cdot \mathbf{s} = 0$ is not satisfied. We train conditional and unconditional DDPM to learn two distributions: the conditional distribution $p(\mathbf{x}|\mathbf{c})$ and the unconditional distribution $p(\mathbf{x}) = p(\mathbf{x})$.

$$\begin{aligned} p(\mathbf{x}|\mathbf{c}) &= \mathcal{N}\left(\mathbf{x}|(-1, -1/\sqrt{3})^T, I\right)^{c_0} \mathcal{N}\left(\mathbf{x}|(1, -1/\sqrt{3})^T, I\right)^{c_1} \mathcal{N}\left(\mathbf{x}|(0, \sqrt{3} - 1/\sqrt{3})^T, I\right)^{c_2} \\ p(\mathbf{x}) &= (p(\mathbf{x}|(1, 0, 0)^T) + p(\mathbf{x}|(0, 1, 0)^T) + p(\mathbf{x}|(0, 0, 1)^T)) / 3 \end{aligned} \quad (57)$$

where \mathbf{c} is a three dimensional one-hot vector.

The guided diffusion model aims to sample from the distribution

$$p(\mathbf{x}|\mathbf{c}; \omega) = \frac{1}{Z(\omega, \mathbf{c})} p(\mathbf{x}|\mathbf{c})^{1+\omega} p(\mathbf{x})^{-\omega} \quad (58)$$

where $Z(\omega, \mathbf{c}) = \int p(\mathbf{x}|\mathbf{c})^{1+\omega} p(\mathbf{x})^{-\omega} d\mathbf{x}$ is the partition function that can be computed with the Monte Carlo method numerically.

We train the denoising neural networks $\epsilon_{\theta}(\mathbf{x}|\mathbf{c}, t)$ and $\epsilon_{\theta}(\mathbf{x}, t)$ for conditional and unconditional neural network on a dataset of 20000 pairs of (\mathbf{x}, \mathbf{c}) . Particularly, The $\epsilon_{\theta}(\mathbf{x}, t)$ is trained as a special case of conditioned $\epsilon_{\theta}(\mathbf{x}|\mathbf{c}, t)$ with $\mathbf{c} = \mathbf{0}$. The characteristic guidance is computed by Alg.2 with $\gamma = 0.05$, $\eta = 0.02$, and $\alpha = 0.99$.

We sample from guided DDPMs using four different ways: the SDE (29), probabilistic ODE (Song et al., 2020b), DDIM (Song et al., 2020a), and DPM++2M (Lu et al., 2022). During sampling, we set $\beta_1 = 1e - 4$, $\beta_2 = 0.02$ and the total time step to be $n = 500$ for SDE and ODE, and $n = 20$ for DDIM and DPM++2M. The sample results are compared with the theoretical reference distribution (58) by assuming the samples from DDPM are Gaussian distributed then computing the KL divergence with the theoretical reference. The results are plotted in Fig.10. Our characteristic guidance outperforms classifier free guidance in all cases with $\omega > 0$.

Fig.10 also shows a significant loss of diversity for classifier free guided ODE samplers when $\omega > 0$. This loss of diversity is corrected by our characteristic guidance, yielding samples that perfectly matches the theoretical reference.

H. Diffusion model for Science: Cooling of Magnet

Guidance, as described in 33, can be conceptualized as a cooling process with the guidance scale ω representing the temperature drop. We demonstrate that the guidance can simulate the cooling process of a magnet around the Curie temperature, at which a paramagnetic material gains permanent magnetism through phase transition. We also demonstrate that non-linear correction for classifier-free guidance is important for correctly characterize the magnet’s phase transition.

The phase transition at the Curie temperature can be qualitatively described by a scalar Landau-Ginzburg model. We consider a thin sheet of 2D magnetic material which can be magnetized only in the direction perpendicular to it. The magnetization of this material at each point is described by a scalar field $\phi(\mathbf{x})$ specifying the magnitude and the direction of magnetization. When ϕ has a higher absolute value, it means that region is more strongly magnetized. Numerically, we discretize $\phi(\mathbf{x})$ into periodic 8×8 grid, with i th grid node assigned with a float number ϕ_i . It is equivalent to say that the magnetization field $\phi(\mathbf{x})$ is represented by 8×8 picture with 1 channel. At any instance, there is a field ϕ describing the current magnetization of our magnet.

Thermal movements of molecules in our magnet gradually change our magnet’s magnetization ϕ from one configuration to another. If we keep track of the field ϕ every second for a long duration, the probability of observing a particular configuration of ϕ is proportional to the Boltzmann distribution

$$p(\phi; T) \propto e^{-\beta H(\phi; T)}, \quad (59)$$

where $\beta H(\phi; T)$ is Hamiltonian at temperature T , assigning an energy to each of possible ϕ . Around the Curie temperature, the Landau-Ginzburg model of our magnet use the following Hamiltonian:

$$\beta H(\phi; T) = K \left(\frac{1}{2} \sum_{\langle i, j \rangle} (\phi_i - \phi_j)^2 + \sum_i \left(\frac{m^2}{2} (T - T_c) \phi_i^2 + \frac{\lambda}{4!} \phi_i^4 \right) \right) \quad (60)$$

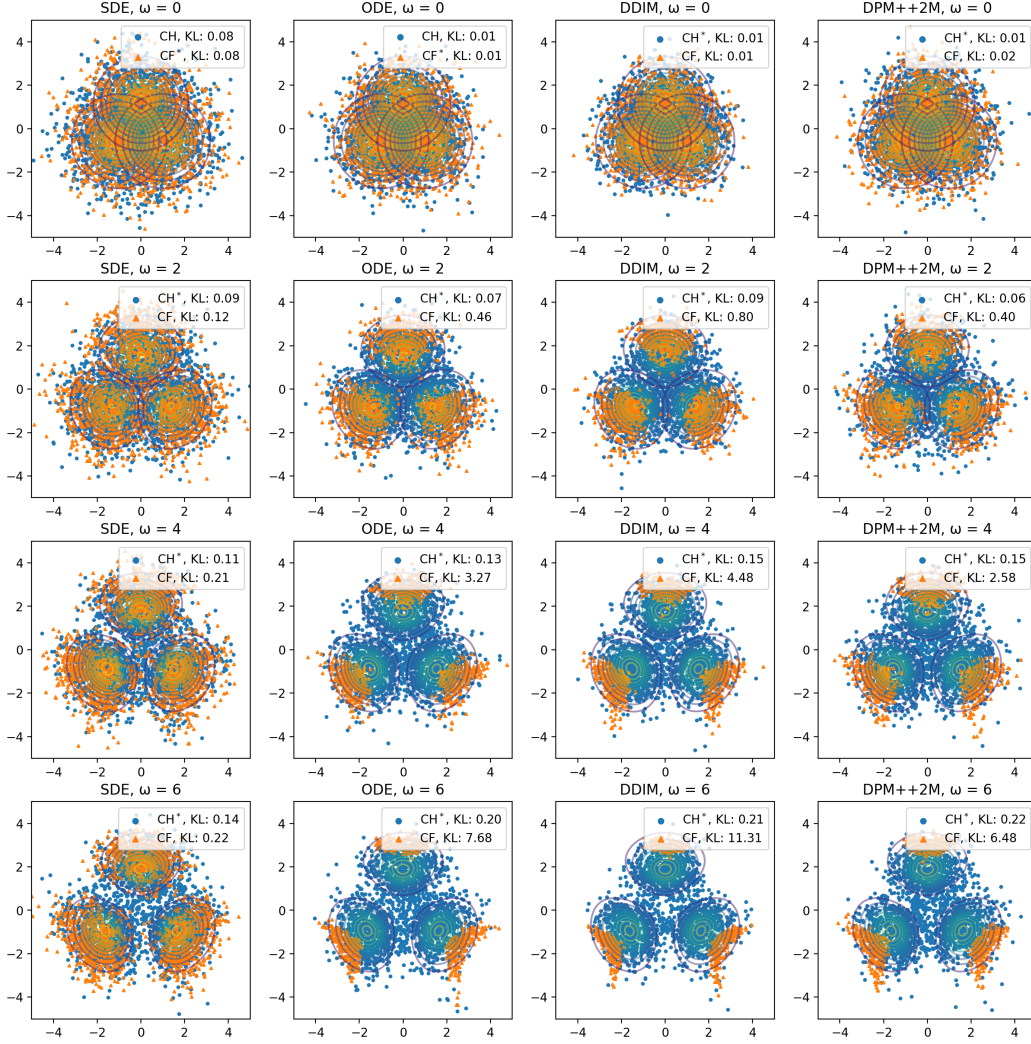


Figure 10. Comparison between characteristic guidance (CH) and classifier free guidance (CF) of DDPM on the mixture of Gaussian experiment. Samples are drawn with various sample methods: SDE, probabilistic ODE, DDIM and DPM++2M. The contours corresponds to the theoretical reference distribution of guided DDPMs in (58).

where $m^2 = 0.1$, $\lambda = 1.0$, $K = 1$ are parameters and $T_c = 200$ is the Curie temperature. The first term sums over adjacent points i and j on the grid, representing the interaction between neighbors. The second term describes self-interaction of each grid. The Landau-Ginzburg model allow us to control the temperature T of magnet using guidance similar to (34)

$$s(\phi; (1 + \omega)T_1 - \omega T_0) = (1 + \omega)s(\phi; T_1) - \omega s(\phi; T_0)$$

where $\omega > 0$ is the guidance scale, $T_0 > T_1$ are two distinct temperature, and $s(\phi; T) = \nabla \log P(\phi; T)$ is the score of the Boltzmann distribution in (59). This means training DDPMs of the magnetization field ϕ at two distinct temperature $T_0 > T_1$ theoretically allow us to sample ϕ at temperatures below T_1 using guidance, corresponding to the cooling of the magnet.

To simulate the cooling of the magnet, we train a conditional DDPM of ϕ for two distinct temperatures $p(\phi|T_0 = 201)$ and $p(\phi|T_1 = 200)$. The dataset consists of 60000 samples at $T_0 = 201$ and 60000 samples at $T_1 = 200$ generated by the Metropolis-Hastings algorithm. Then we sample from the trained DDPM using classifier-free guidance in (35) and

characteristic guidance in (6)

$$\begin{aligned} \epsilon_{CF}(\mathbf{x}|(1 + \omega)T_1 - \omega T_0, t_i) &= (1 + \omega) \epsilon_{\theta}(\mathbf{x}|T_1, t_i) - \omega \epsilon_{\theta}(\mathbf{x}|T_0, t_i) \\ \epsilon_{CH}(\mathbf{x}|(1 + \omega)T_1 - \omega T_0, t_i) &= (1 + \omega) \epsilon_{\theta}(\mathbf{x} + \omega \Delta \mathbf{x}|T_1, t_i) - \omega \epsilon_{\theta}(\mathbf{x} + (1 + \omega) \Delta \mathbf{x}|T_0, t_i). \end{aligned} \tag{61}$$

The characteristic guidance is computed with Alg.2 with $\gamma = 0.01$, $\eta = 0.1$, and $\alpha = 0.999$. Samples from the guided DDPM is treated approximately as samples at temperature $T = (1 + \omega)T_1 - \omega T_0$.

We sample from guided DDPMs using four different ways: the SDE (29), probabilistic ODE (Song et al., 2020b), DDIM (Song et al., 2020a), and DPM++2M (Lu et al., 2022). During sampling, we set $\beta_1 = 1e - 4$, $\beta_2 = 0.015$ and the total time step to be $n = 1000$ for SDE and ODE, and $n = 20$ for DDIM and DPM++2M. For each temperature, we generate theoretical reference samples from the Boltzmann distribution in (59) with the Metropolis-Hastings algorithm. The negative log-likelihood (NLL) of samples of DDPM is computed as their mean Landau-Ginzburg Hamiltonian, subtracting the mean Landau-Ginzburg Hamiltonian of samples of the Metropolis-Hastings algorithm. The histogram of the mean value of the magnetization ϕ field values are plotted in Fig.11.

A phase transition occurs at the Curie temperature $T_c = 200$. Above the Curie temperature, the histogram of the mean magnetization has one peak centered at 0. At a certain instance, the thermal movements of molecules in our magnet may lead to a non-zero net magnetization, but the average magnetization over a long time is still zero, corresponding to a paramagnetic magnet. Below the Curie temperature, the histogram of the mean magnetization has two peaks with non-zero centers. Jumping from one peak to another at this case is difficult because the thermal movements of molecules only slightly change the mean magnetization and are insufficient to jump between peaks. This leads to a non-zero average magnetization over a long time and corresponds to a permanent magnet. Both classifier-free and characteristic guidance generate accurate samples above the Curie temperature where the DDPM is trained. However, the characteristic guidance generates better samples below the Curie temperature and has better NLL. Moreover, samples of characteristic guidance have well-separated peaks while samples of classifier-free guidance are not. This means the characteristic guidance has a better capability to model the phase transition.

I. Cifar 10

J. Latent Diffusion Model

Characteristic Guidance: Non-linear Correction for Diffusion Model at Large Guidance Scale

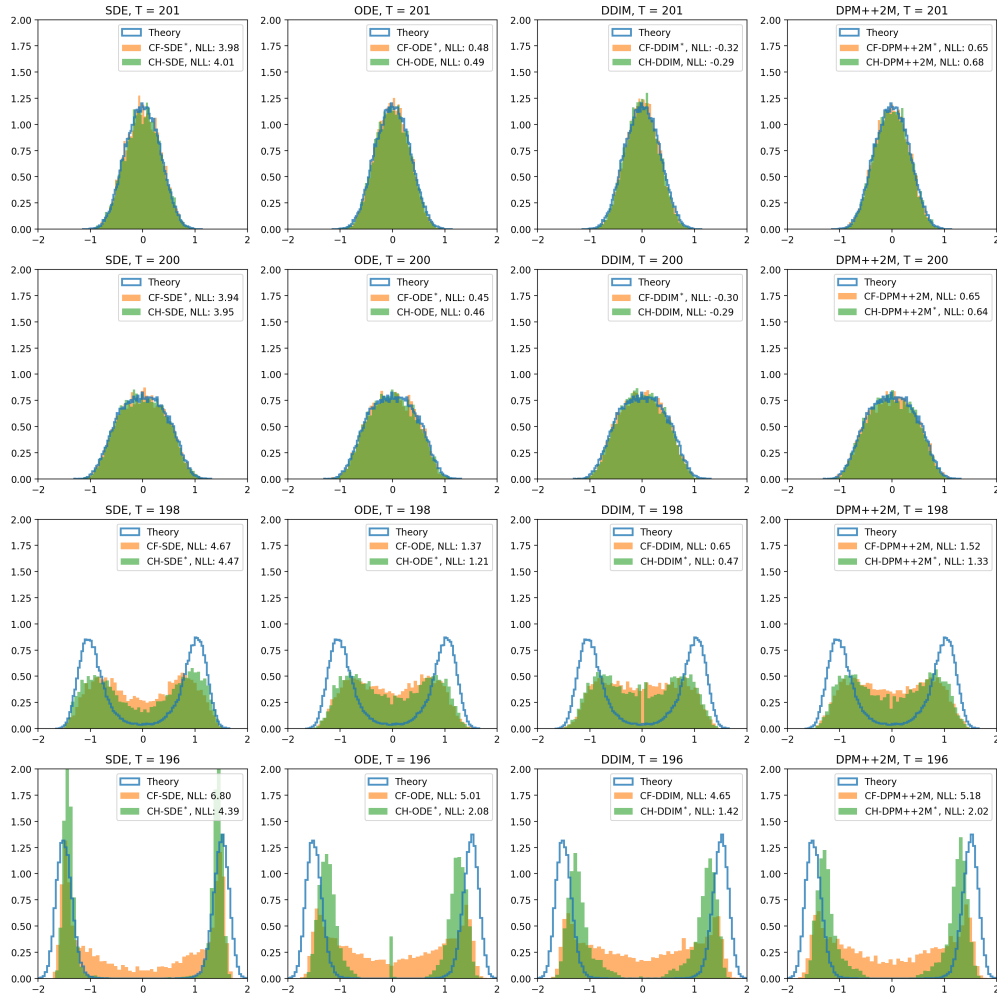


Figure 11. The histogram of the mean magnetization of the Landau-Ginzburg magnet model around the Curie temperature $T = 200$. The magnetization fields are generated by classifier-free and characteristic guidance. The characteristic guidance generates better samples below the Curie temperature $T = 200$ and has better NLL.

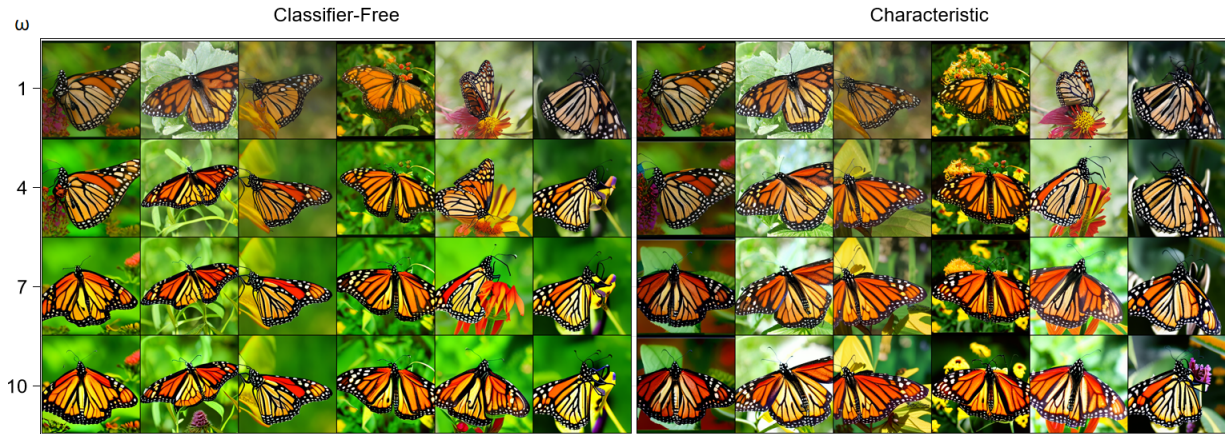


Figure 12. Comparative visualization of butterfly (323) images generated from latent diffusion model using Classifier Free Guidance (CF) versus Characteristic Guidance (CH).

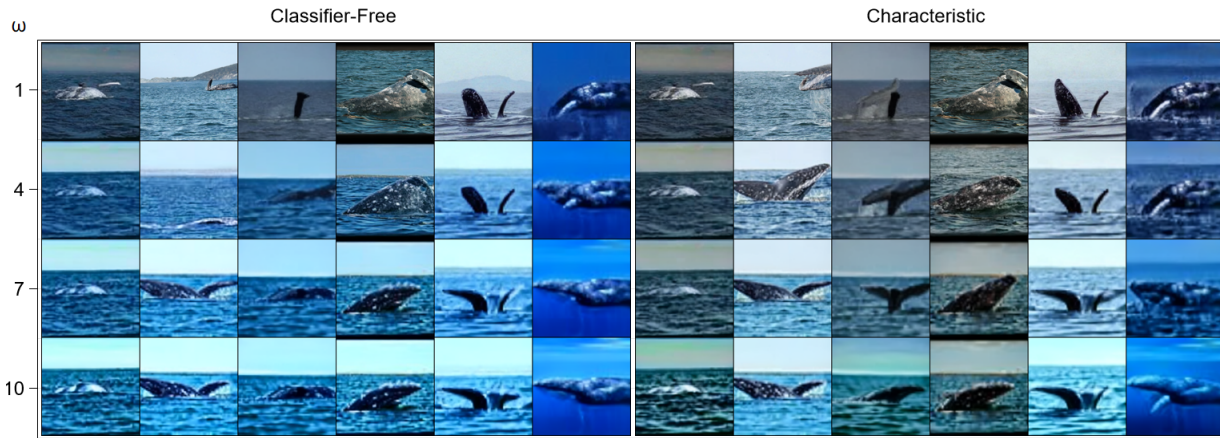


Figure 13. Comparative visualization of whale (147) images generated from latent diffusion model using Classifier Free Guidance (CF) versus Characteristic Guidance (CH).

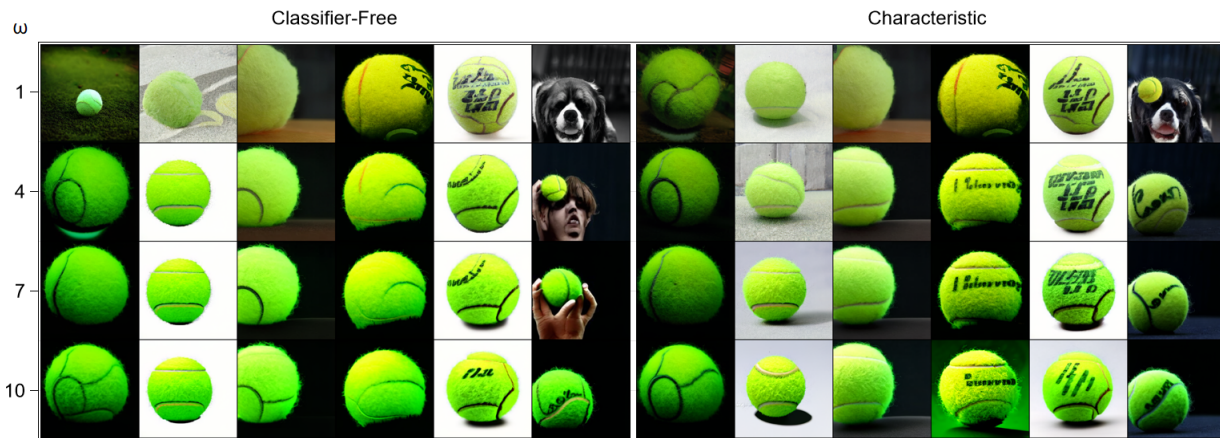


Figure 14. Comparative visualization of butterfly (852) images generated from latent diffusion model using Classifier Free Guidance (CF) versus Characteristic Guidance (CH).

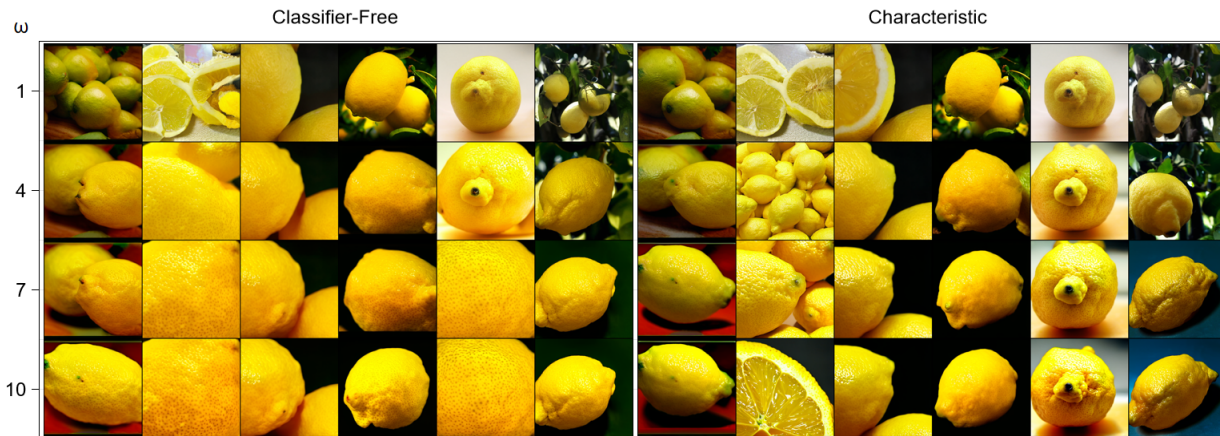


Figure 15. Comparative visualization of lemon (147) images generated from latent diffusion model using Classifier Free Guidance (CF) versus Characteristic Guidance (CH).



Figure 16. Comparative visualization of barn (425) images generated from latent diffusion model using Classifier Free Guidance (CF) versus Characteristic Guidance (CH).

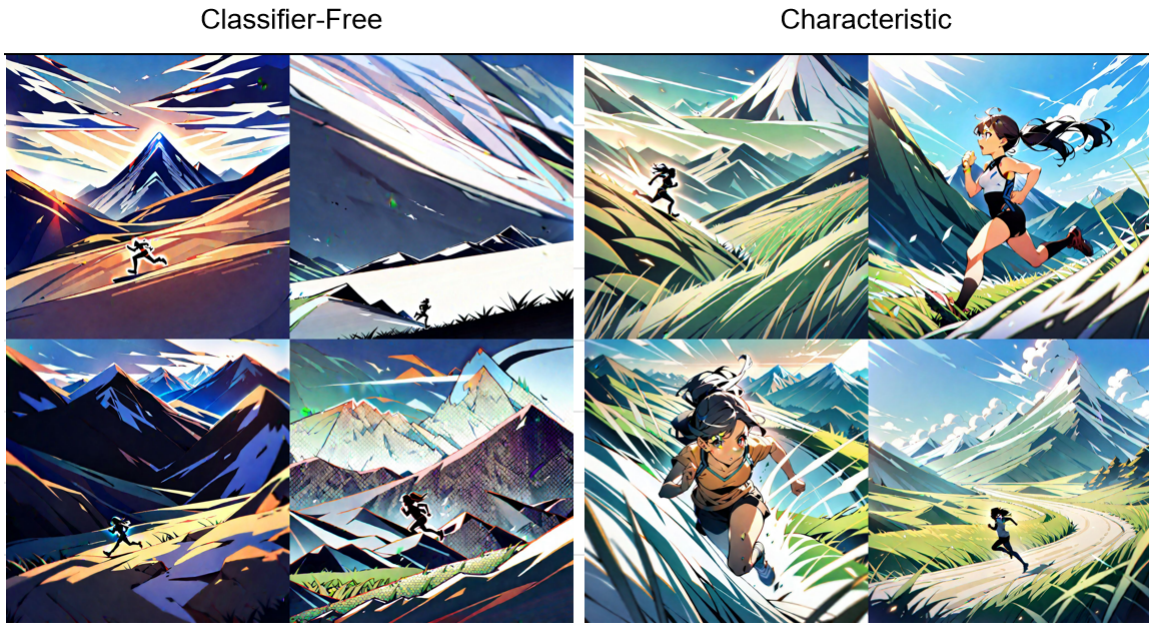


Figure 17. 1girl, running, mountain, grass. Comparative visualization of images generated from Stable Diffusion WebUI using Classifier Free Guidance versus Characteristic Guidance. Infotext of image (batch size 4, with the Characteristic Guidance Web UI extension): 1girl, running, mountain, grass. Negative prompt: low quality, worst quality. Steps: 30, Sampler: UniPC, CFG scale: 30, Seed: 0, Size: 1024x1024, Model hash: 1449e5b0b9, Model: animagineXLV3_v30, CHG: "{RegS: 5, RegR: 1, MaxI: 50, NBasis: 1, Reuse: 0, Tol: -4, ItESS: 1, ASpeed: 0.4, AStrength: 0.5, AADim: 2, CMode: 'More ControlNet'}", Version: v1.7.0

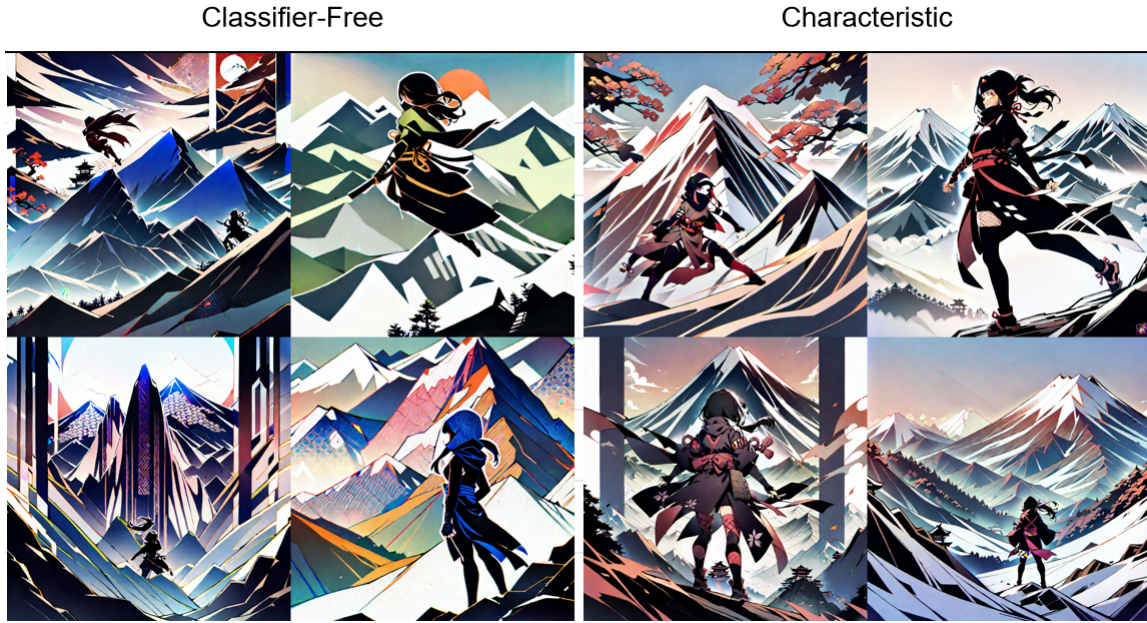


Figure 18. 1girl, ninja, mountain. Comparative visualization of images generated from Stable Diffusion WebUI using Classifier Free Guidance versus Characteristic Guidance. Infotext of image (batch size 4, with the Characteristic Guidance Web UI extension): *1girl, ninja, mountain, Negative prompt: low quality, worst quality, Steps: 30, Sampler: UniPC, CFG scale: 30, Seed: 0, Size: 1024x1024, Model hash: 1449e5b0b9, Model: animagineXLV3_v30, CHG: "{RegS: 5, RegR: 1, MaxI: 50, NBasis: 1, Reuse: 0, Tol: -4, IteSS: 1, ASpeed: 0.4, AStrength: 0.5, AADim: 2, CMode: 'More ControlNet'}", Version: v1.7.0*

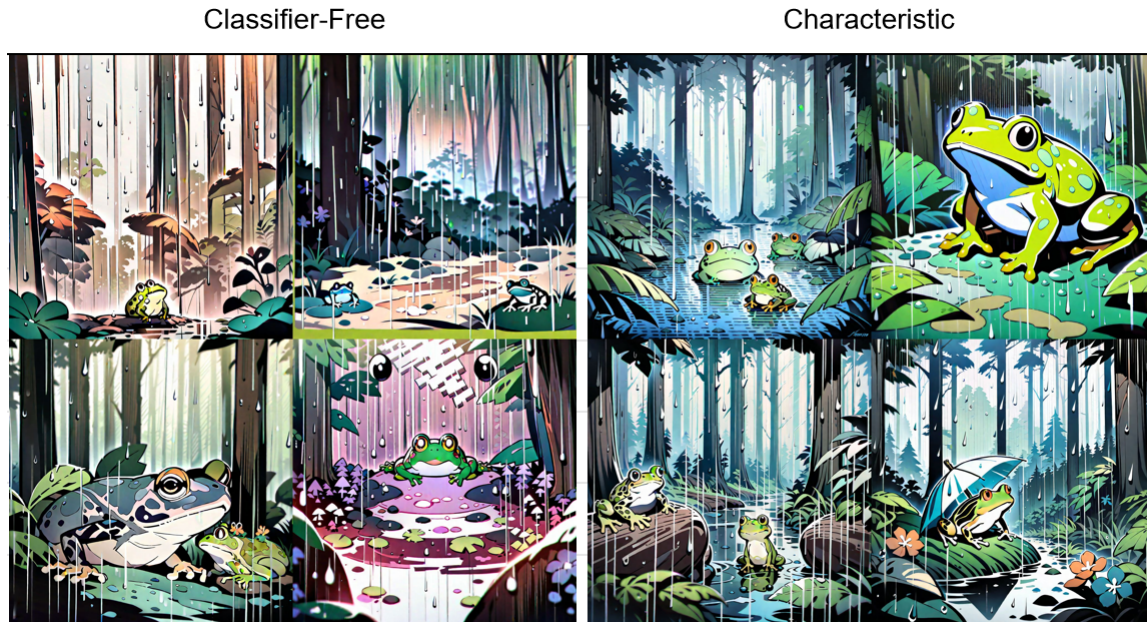


Figure 19. frog, forest, rain. Comparative visualization of images generated from Stable Diffusion WebUI using Classifier Free Guidance versus Characteristic Guidance. Infotext of image (batch size 4, with the Characteristic Guidance Web UI extension): *frog, forest, rain, Negative prompt: low quality, worst quality, Steps: 30, Sampler: UniPC, CFG scale: 30, Seed: 0, Size: 1024x1024, Model hash: 1449e5b0b9, Model: animagineXLV3_v30, CHG: "{RegS: 5, RegR: 1, MaxI: 50, NBasis: 1, Reuse: 0, Tol: -4, IteSS: 1, ASpeed: 0.4, AStrength: 0.5, AADim: 2, CMode: 'More ControlNet'}", Version: v1.7.0*



Figure 20. battleship, space, moon. Comparative visualization of images generated from Stable Diffusion WebUI using Classifier Free Guidance versus Characteristic Guidance. Infotext of image (batch size 4, with the Characteristic Guidance Web UI extension): *battleship, space, moon, Negative prompt: low quality, worst quality, Steps: 30, Sampler: UniPC, CFG scale: 30, Seed: 0, Size: 1024x1024, Model hash: 1449e5b0b9, Model: animagineXLV3_v30, CHG: "{RegS: 5, RegR: 1, MaxI: 50, NBasis: 1, Reuse: 0, Tol: -4, IteSS: 1, ASpeed: 0.4, AStrength: 0.5, AADim: 2, CMode: 'More ControlNet'}*", Version: v1.7.0